PNAS
www.pnas.org

Supplementary Information for

Unveiling Causal Interactions in Complex Systems

Authors: Stavros K. Stavroglou[1*], Athanasios A. Pantelous[2*], H. Eugene Stanley[3,4*], Konstantin M. Zuev[5]

Affiliations: [1]Department of Mathematical Sciences, University of Liverpool, Liverpool, L697ZL, UK. [2]Department of Econometrics and Business Statistics, Monash University, Clayton VIC 3800, Australia. [3]Center for Polymer Studies, Boston University, Boston, MA 02215, USA. [4]Department of Physics, Boston University, Boston, MA 02215, USA. [5]Department of Computing and Mathematical Sciences, California Institute of Technology, Pasadena, CA 91125**,** USA.

*****corresponding authors

Stavros K. Stavroglou: stavros.stavroglou@liverpool.ac.uk
Athanasios A. Pantelous: athanasios.pantelous@monash.edu
H. Eugene Stanley: hes@bu.edu

This PDF file includes:

Causal interaction in practice.

We propose a novel methodology (see Methods in the main text for the details) for studying the interdependencies which comprise the hidden structures of complex systems. We draw motivation from three diverse areas of research: firstly, we consider the problem of ecosystem oversight in a desert region where an exotic plant species invades the system. Secondly, we look at the causal interactions of EEG activity to diagnose hidden patterns in the brain of an alcoholic person. Finally, we apply our method in a simple yet prudent way to reveal the underlying causal structure in a set of banking derivatives.

1. Notational Information

Before the theoretical methodology is developed to reveal causal networks, it is necessary to introduce the following notation:

Variable	Description
$\Omega \in \mathbb{R}^m$	A dynamical system evolving in an m-dimensional state space.
$M \in \mathbb{R}^E$	The attractor of Ω consisting of all trajectories and possible states $\underline{\mu}(t)$ of the system. M is an E-dimensional attractor embedded in an m-dimensional state space ($E \leq m$). The state space contains the manifold and its dynamics and consists of the original E Cartesian coordinates (fundamental variables) of the system.
$\underline{\mu}(t) \in \mathbb{R}^E$	The point (vector) on M representing the state of the system at time t.
$X(t) \in \mathbb{R}$	State variables (time series) of the dynamical system Ω that operate as a function which maps points from Ω's attractor M to a real-valued scalar. X may correspond to Cartesian coordinates of the actual E-dimensional state space containing M.
$t \in \mathbb{N}$	Denotes time measured in discrete steps $t_1, t_2, t_3, \ldots$ of X's temporal evolution.
$L \in \mathbb{N}$	The time series length, also called the library of the time series.
$E \in \mathbb{N}$	The embedding dimension of the attractor.
$\tau \in \mathbb{N}$	The time lag we use to reconstruct a shadow attractor.
$M_X \in \mathbb{R}^E$	The shadow attractor reconstructed using time lags of $X(t)$.
$\underline{x}(t) \in \mathbb{R}^E$	The points (vectors) of M_X corresponding to the state of the system at time t.
$h \in \mathbb{N}$	The prediction horizon h steps ahead of current time t.
$L_1 \in \mathbb{R}$	The Manhattan distance measured as $d_1\left(\underline{x}(t_1), \underline{x}(t_2)\right) = \sum_{i=1}^{E} \lvert \underline{x}(t_1^i) - \underline{x}(t_2^i) \rvert$
$L_2 \in \mathbb{R}$	The Euclidean distance measured as $d_2\left(\underline{x}(t_1), \underline{x}(t_2)\right) = \sqrt{\sum_{i=1}^{E} (\underline{x}(t_1^i) - \underline{x}(t_2^i))^2}$
$D_X \in \mathbb{R}^{E-1}$	The distance matrix according to some metric (e.g. L_1 or L_2).
$NN_{\underline{x}(t)} \in \mathbb{R}^{E-1}$	The nearest neighbors of $\underline{x}(t)$ according to D_X.
$S_{\underline{x}(t)} \in \mathbb{R}^{E-1}$	The vector of successive percentage changes of $\underline{x}(t)$.
$\hat{S}_{\underline{x}(t+h)} \in \mathbb{R}^{E-1}$	The vector of successive percentage changes of $\underline{x}(t+h)$.
$P_{\underline{x}(t)} \in \mho^E$	The current pattern of $\underline{x}(t)$. For the trivial case of $E = 2$, we have three possible patterns: ↗, ➡, ↘.
$\hat{P}_{\underline{x}(t+h)} \in \mho^E$	The estimated forecasted pattern of the affected variable, extracted as the signature of $\hat{S}_{\underline{x}(t+h)}$.
$PC[P_X, P_Y, t] \in \mho^E$	The pattern causality (PC) matrix which is a 3D array with dimensions $(3^{E-1}, 3^{E-1}, L)$ which models the influence strength.
$P_X \parallel P_Y$	$\parallel$ denotes that the patterns are the same. See main diagonal (blue) of PC matrix.

$P_X \perp P_Y$	$\perp$ denotes that the patterns are opposites. See anti-diagonal (red) of PC matrix.
$P_X \nparallel P_Y$	$\nparallel$ denotes that the patterns are neither the same nor opposites. See all other elements (purple) of PC matrix.

2. Extensive Algorithm Plug-ins

Node-level statistics:

- *degree* is the number of outgoing and incoming links in a given node (Hakimi 1962). Out-degree denotes the influence exerted directly on other nodes and in-degree denotes the influence received directly from other nodes.
- *closeness* measures the reciprocal of how many steps are required to access every other node from a given node (Bavelas 1950). High out-closeness means that a node might spill its influence over onto further nodes (apart from its direct links). Similarly, high in-closeness suggests that a node might receive indirect influences from nodes beyond its immediate proximity.
- *betweenness* is (roughly) defined as the number of geodesics (shortest paths) going through a node (Freeman 1977). High betweenness in our framework suggests that the nodes in question might enable the propagation of indirect influences across the whole network.
- *eigenvector* measures the influence a node has on a network. If a node is pointed to by many nodes (which have high eigenvector centrality), then that node will also have high eigenvector centrality (Newman 2016). Practically speaking, a high-eigenvector node in an interdependencies network indicates a time series which is at the top of the influential hierarchy.
- *strength* is the aggregation of the weights of the links from and to the node (weighted degree) (Barrat et al. 2004). Out-strength denotes the weighted influence exerted directly on other nodes and in-strength denotes the weighted influence received directly from other nodes. Weights, here, are obtained from Eq. (11).
- *node diversity* measures the diversity of a given node according to some node property (e.g. degree) (Eagle et al. 2010). In our framework, we can use this statistic to identify time series with strange or uncommon interdependencies structures.

Link statistics:

link persistence measures the overall weight of a given link from node X to node Y by aggregating cumulatively across time in order to rank time series interdependencies by strength and persistence (Stavroglou et al 2017).

Neighborhood-level statistics:

- *rich club coefficient* measures the extent to which nodes with many links also connect to each other (Zhou and Mondragon 2004). In our framework, we can extract two types of rich clubs: (a) one considering only outgoing links, allowing us to locate which time series constitute the "main driving core" of the system, and (b) another considering only incoming links, allowing us to locate which time series constitute the "main affected core" of the system. We refer to these rich clubs collectively as "hyper-active cores".
- *k-core decomposition*: the k-core of a network is a maximal subgraph in which each node has at least degree k. The coreness of a node is k if it belongs to the k-core but not to the $(k+1)$-core (Seidman 1983). This statistic can give us the detailed hierarchical structures of influence exertion (considering out-degree) and influence absorption (considering in-degree).
- *community detection* identifies sets of nodes such that each set of nodes is densely connected internally (Porter et al. 2009). Communities in interdependencies networks suggest groups of time series which are almost independent from the time series outside their community.

Network-wide statistics:

- *aggregate intensity* is simply the summation of all the link's weights, as calculated from Eq. (11). It denotes the overall influence at play in a given network and can be used to compare different networks in a straightforward manner.
- *centralization* measures how central the most central node is in relation to how central all the other nodes are (Freeman 1978). Centrality is measured according to the aforementioned node-level statistics. A highly centralized (in terms of out-degree for

example) causal network suggests the existence of a time series acting as a singularity of influence over the whole set of time series.

- *components* measure the number of weakly connected components (Hopcroft and Tarjan 1973). The higher is the number of components, the less global the influence exerted can be considered, meaning that the time series under study cluster in smaller groups.
- *density* measures how densely connected the network is (Coleman and More 1983). High density of a causal network suggests intense bursts of influence among all its time series.
- *articulation* measures the percentage of articulation nodes (Barnes and Harary 1983). Such nodes (in our case, time series), if removed, disconnect the network, meaning they probably play a connector role among densely interdependent time series. Articulation nodes are, in brief, bridges of influence.
- *average path length* measures the average number of nodes needed for each node to reach every other node (West 1996). The lower it is, the more direct are the interdependencies in a system.
- *clustering coefficient* measures the degree to which nodes in a graph tend to cluster together (Luce and Perry 1949). High clustering suggests many triangles of interdependencies.
- *entropy*: the extent to which the frequency distribution of a node property (e.g. degree centrality) is uniform (Shannon 1948). Picking a node-level statistic and using entropy over its distribution across all nodes allows us to understand how diverse (low entropy) or uniform (high entropy) is the specific influence characteristic in our system.
- *modularity (walktrap)* measures the strength of division of a network into communities. High modularity suggests dense connections between the nodes within communities but sparse connections between nodes in different communities. The walktrap algorithm works well with directed networks which are the de facto product of pattern causality (Pons and Latapy 2006).
- *assortativity coefficient* takes positive values if similar nodes (based on a node property) tend to connect to each other, and negative values otherwise (Newman 2002).

If a causal network has a high assortativity coefficient, then it means that time series of similar interdependencies cluster together.

- *scale-free property* is the property of a network whose degree distribution follows a power law, at least asymptotically (Price 1965). In our framework, a network being scale-free in terms of out-degree would suggest the existence of few time series with highly influential connectivity and many with weak influential connectivity. Analogous conclusions would stem from a network being scale-free in terms of in-degree.
- *small world property* characterizes a network in which most nodes are not neighbors of one another, but the neighbors of any given node are likely to be neighbors of each other and most nodes can be reached from any other node in a small number of hops or steps (Watts and Strogatz 1998).

3. Big "O" Complexity

Our method is computationally efficient for long time series (large L). Note that our algorithm receives as inputs E and τ and the pair of time series under consideration. τ does not affect the complexity of the algorithm. Therefore, the only parameters that impact our method are the time series length L and its embedding dimension E. The higher are L and/or E, the longer it will take for the distance matrices D_X and D_Y to be calculated. A simple trick to avoid the mass calculations of D_X and D_Y at each iteration (for every time step) is to compute them at the beginning, before any iteration, once and for all. This way, to extract the candidate neighbors of a point $\underline{x}(t)$, we only need the $D_X[t, 1{:}\,(t-1)]$ part of D_X (same for D_Y). Computing D_X and D_Y costs L^2E for each and the iteration part of the main algorithm is of order $O(L)$.

The total cost of our algorithm is of order $O(L^2E + L)$ with the main bulk of the calculations being that of the initial distance matrices.

Below, we lay out the analytical complexity for every step of our algorithm:

Step 1: Reconstructing the shadow attractors M_X and M_Y is of order $O(L)$ and calculating D_X and D_Y is of order $O(L^2E)$.

Steps 2 to 6 are performed for every t in the time series. Therefore, the loop including them is of order $O(L)$.

Step 2: Parsing every row (which corresponds to finding the nearest neighbors for each point $\underline{x}(t)$) in D_X is of order $O(E+1)$.

Step 3: The extraction of $\hat{P}_{\underline{y}(t+h)}$ is trivially of order $O(E+1)$.

Step 4: Retrieving $P_{\underline{x}(t)}$ is of order $O(E)$.

Step 5: Retrieving the real $P_{\underline{y}(t+h)}$ pattern is of order $O(E)$.

Step 6: Filling the PC pattern into the pattern matrix is a procedure of order $O(1)$.

4. Synthetic Interdependencies Validation

The purpose of this application is to validate the capacity of our method to discern positive, negative and dark interdependencies. We use the following model to generate a synthetic influence from a time series X to a time series Y:

$$X(t) = X(t-1) + S_{\underline{x}(t)}, \qquad S_{\underline{x}(t)} \in \mathbb{R}^{E-1}$$
$$Y(t) = Y(t-1) + \alpha(X(t), S_{\underline{x}(t)}, \kappa),$$

where

$$\alpha\big(X(t), S_{\underline{x}(t)}, \kappa\big) = \begin{cases} S_{\underline{y}(t)} : P_{\underline{y}(t)} \parallel P_{\underline{x}(t)}, & \kappa = "positive" \\ S_{\underline{y}(t)} : P_{\underline{y}(t)} \perp P_{\underline{x}(t)}, & \kappa = "negative" \\ S_{\underline{y}(t)} : P_{\underline{y}(t)} \nparallel P_{\underline{x}(t)}, & \kappa = "dark" \end{cases}$$

We have $S_{\underline{x}(t)}$ following a uniform distribution and $S_{\underline{y}(t)}$ taking values according to the function $\alpha\big(X(t), S_{\underline{x}(t)}, \kappa\big)$ described above. We run 100,000 simulations separately for each of the three types of influence (positive, negative, dark) we want to synthesize. For this application, we use $E = 2, \tau = 1$ and $h = 1$.

Synthetic influences generation

To simulate a positive influence, for each time step *t* we use a uniform *random number generator* (RNG) with the following settings: 90% chance that κ = "positive", 5% chance that κ = "negative" and 5% chance that κ = "dark". The reason we do this is to allow our model to produce mixed influence types in order to make it more realistic and test our method in a more robust setting.

Similarly, we simulate a negative influence by giving the RNG the following settings: 5% chance that κ = "positive", 90% chance that κ = "negative" and 5% chance that κ = "dark". A dark influence is generated as follows: 5% chance κ = "positive", 5% chance κ = "negative" and 90% chance κ = "dark".

Recording chains of consecutive influences of a single type of influence

After producing 100,000 simulations for each type of influence, we record consecutive incidents or chains (up to a length of 15) of the same type we want to test (e.g. for positive influence simulations we consider only positive instances of influence etc.), and we record in columns A, C and E of Table S2 the percentage our toy model generated (for each chain length). For example, in the positive simulations, positive chains of length 2 were recorded in 85.742% (Col. A, Chain 2 row) of cases in the 100,000 simulations, meaning that the remaining 14.258%are instances of negative and dark influence.

Measuring the accuracy of our algorithm in detecting the target type of influence

Once we have determined the percentages of chains of interest, we run our method in order to gauge the extent to which it can detect the actual type of influence for chains of lengths up to 15. As we can observe from Table 2, for the positive influence test (Col. B) our algorithm reaches 93.5685% accuracy in terms of single positive instances (chain length = 1) and dwindles smoothly to a floor of 82.9421% accuracy for positive chains of length 15. For the case of negative simulations, our method performs equally well (Col. D), starting from 93.4461% for single negative instances and ending up at an 84.7194% accuracy level for negative chains of length 15. Lastly, in the case of dark simulations, our algorithm starts

with an equally high accuracy rate of 91.2583% for single dark instances. Its accuracy does dwindle more as we require longer chains, but still reaches an accuracy of 66.9014% for long dark sequences (chain length 15).

Overall, we observe that our method detects chains of the same type of influence with very high accuracy, implying it is ready to be deployed in real-world applications (see following section) where the requirements for consecutive predictions may not be as demanding as we have tested for here.

Table S1. Results on synthetic interdependencies data. Columns A, C and E record the percentage of interactions produced of the type the model originally was i.e. column A records percentage of positive couplings that emerged from the positive setup (chance of positive coupling 90%). Columns B, D and F record the accuracy our algorithm had on predicting the type of causality (positive for positive setup and so on) we expected to capture.

Col. ID	**A**	**B**	**C**	**D**	**E**	**F**
Chain	Synthetic Positive Influence % (over all simulations), κ="positive", chance: 90%	Positive Influence % detected (over Col. A)	Synthetic Negative Influence % (over all simulations), κ="negative", chance: 90%	Negative Influence % detected (over Col. C)	Synthetic Dark Influence % (over all simulations), κ="dark", chance: 90%	Dark Influence % detected (over Col. E)
1	0.90316	0.935685	0.90324	0.934461	0.9037	0.912583
2	0.85742	0.919376	0.85746	0.91795	0.85699	0.870118
3	0.81369	0.903037	0.81398	0.906387	0.81442	0.827617
4	0.77255	0.895689	0.7735	0.896612	0.7735	0.801096
5	0.73397	0.900327	0.73429	0.897846	0.73385	0.767928
6	0.69738	0.887563	0.69688	0.892708	0.69627	0.72395
7	0.66196	0.890719	0.66128	0.881897	0.66037	0.723277
8	0.62912	0.877747	0.62865	0.874394	0.62733	0.641479
9	0.59743	0.887244	0.59627	0.880292	0.59626	0.664063
10	0.56698	0.873929	0.56675	0.873171	0.56595	0.619247
11	0.53872	0.86402	0.53866	0.853904	0.53778	0.669014
12	0.51274	0.845556	0.51236	0.862482	0.51095	0.641975
13	0.4865	0.846154	0.48578	0.850306	0.48547	0.62500
14	0.46157	0.842636	0.46121	0.847194	0.46138	0.53125
15	0.43877	0.829421	0.43796	0.822115	0.43917	0.529412

5. Supplementary Information for the Applications

Details of the desert ecosystem

In order to reconstruct the ecosystem's causal network, we took the common time span for which data were available in all four categories, namely, from 1993 to 2009. We implemented our method on time series constructed from 32 data inputs (Table S2), with $E = 2, \tau = 1$ and $h = 0$. We used $h = 0$ because the quantities were averaged to a yearly basis from varying time frequencies. Thus, for this application, we wanted to examine the concurrent interactions in the system from year to year and not the predictions. To keep the strongest interactions, we filtered the network links with the "Maximum Spanning Tree" algorithm (Hu 1961) using the weights retrieved from Eq. (11) of our method. As a result, we plotted six periods of interest (Figure 1) in order to depict the ecosystem's synergies.

Table S2. Species in the Chihuahuan Desert ecosystem in Arizona

Weather	**Rodents**	**Plants**	**Ants**
Temperature	*Ammospermophilus harrisi*	*Astragalus nuttallianus*	*Conomyrma bicolor*
Precipitation	*Dipodomys merriami*	*Cassia bauhinoides*	*Conomyrma insane*
	Dipodomys ordii	*Ephedra trifurca*	*Iridomyrma pruinosum*
	Neotoma albigula	*Eriastrum diffusum*	*Novomessor cockerelli*
	Onychomys torridus	*Erodium cicutarium*	*Pheidole sitarches*
	Peromyscus eremicus	*Gutierrezia sarothrae*	*Pheidole xerophila*
	Chaetodipus penicillatus	*Lesquerella gordoni*	*Pogonomyrmex desertorum*
	Reithrodontomys megalotis	*Perezia nana*	*Solenopsis sp.*
	Spermophilus spilosoma	*Plantago patagonica*	*Solenopsis xyloni*
		Solanum eleagnifolium	
		Phemeranthus angustissimum	
		Phemeranthus aurantiacus	

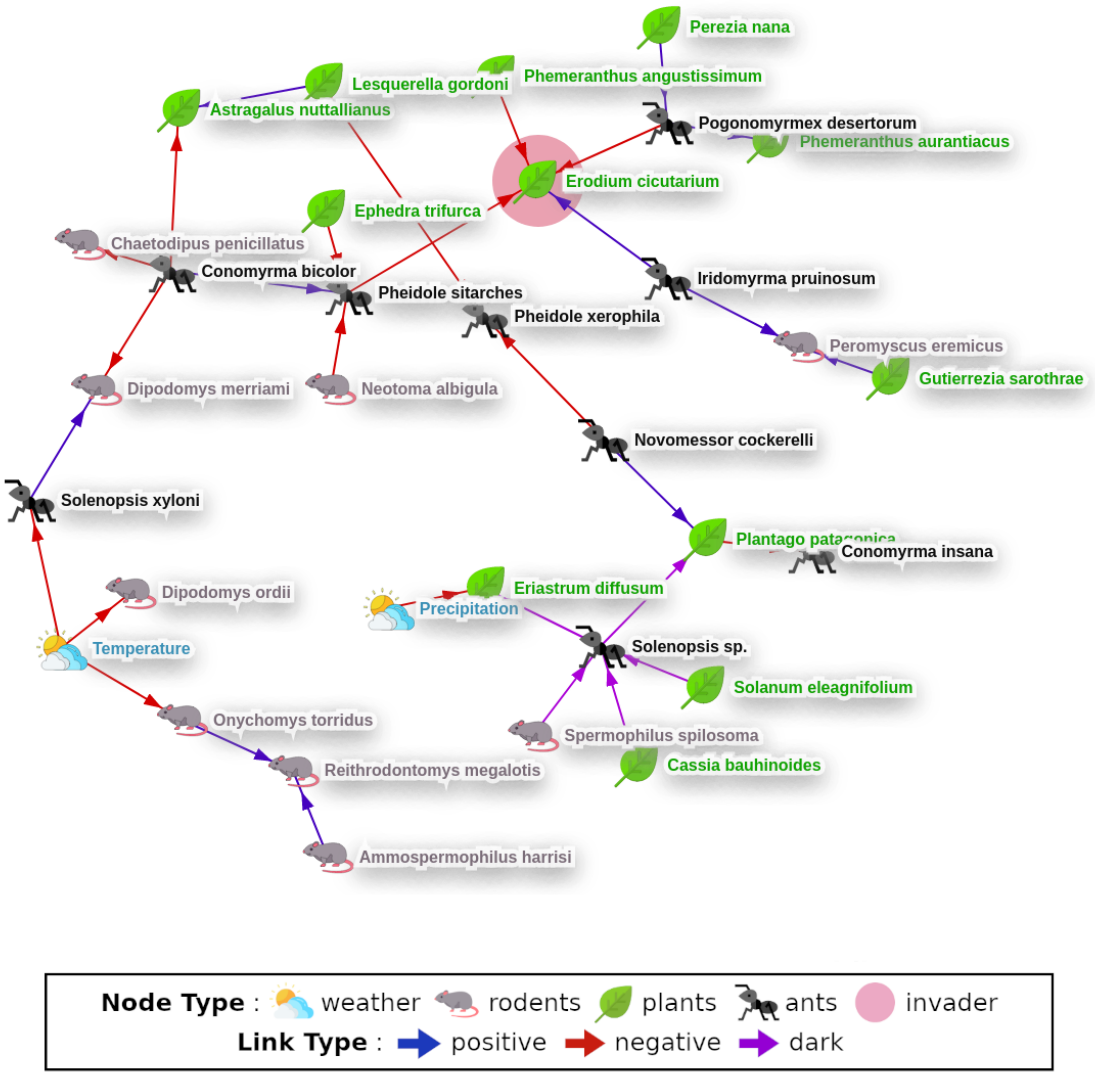

Figure S1. Aggregate causal network before the "aggression" of Erodium cicutarium. The node icon is representative of the node's type (ants, plants, rodents, weather). The link color denotes type of causality (blue for positive, red for negative and purple for dark).

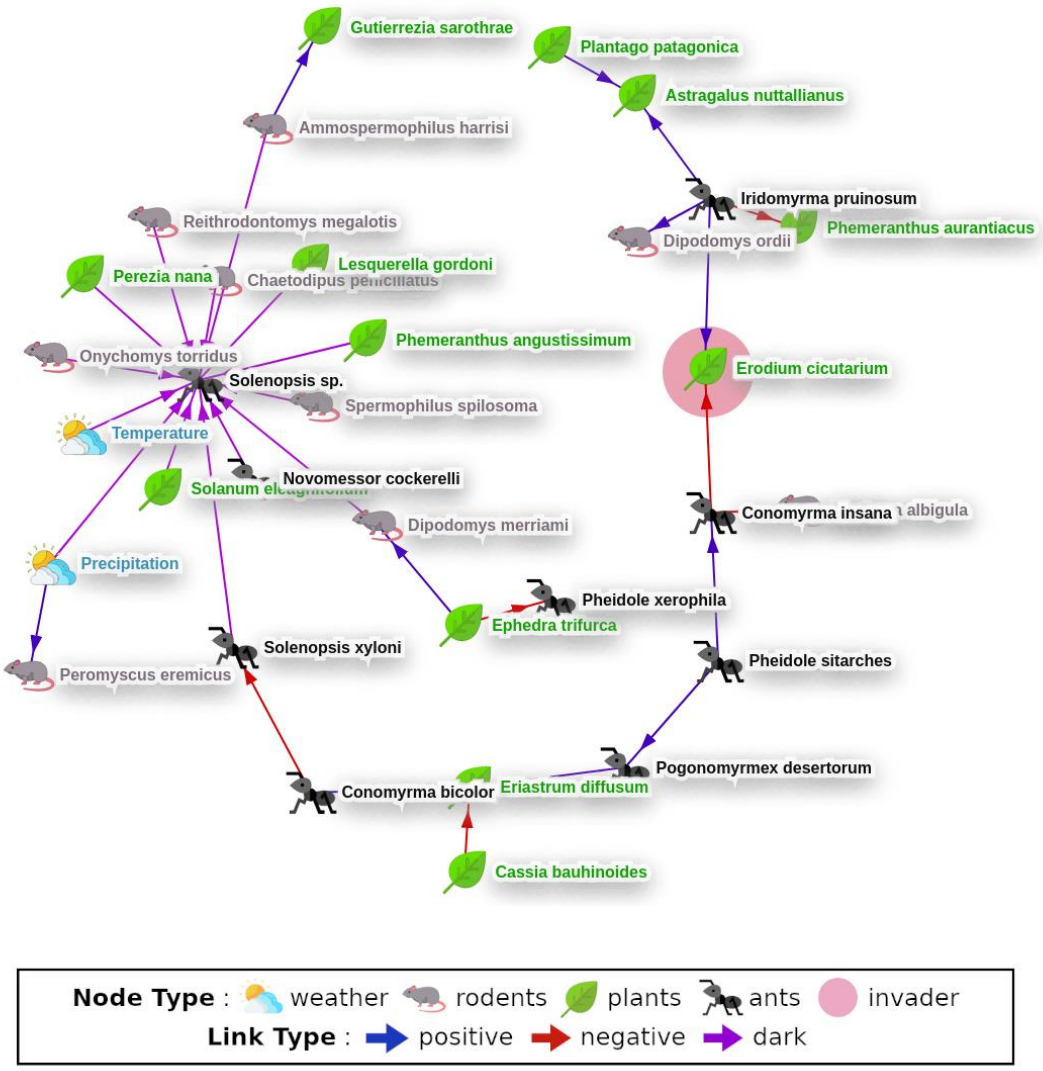

Figure S2. Aggregate causal network during the invasion period of Erodium cicutarium. The node icon is representative of the node's type (ants, plants, rodents, weather). The link color denotes type of causality (blue for positive, red for negative and purple for dark).

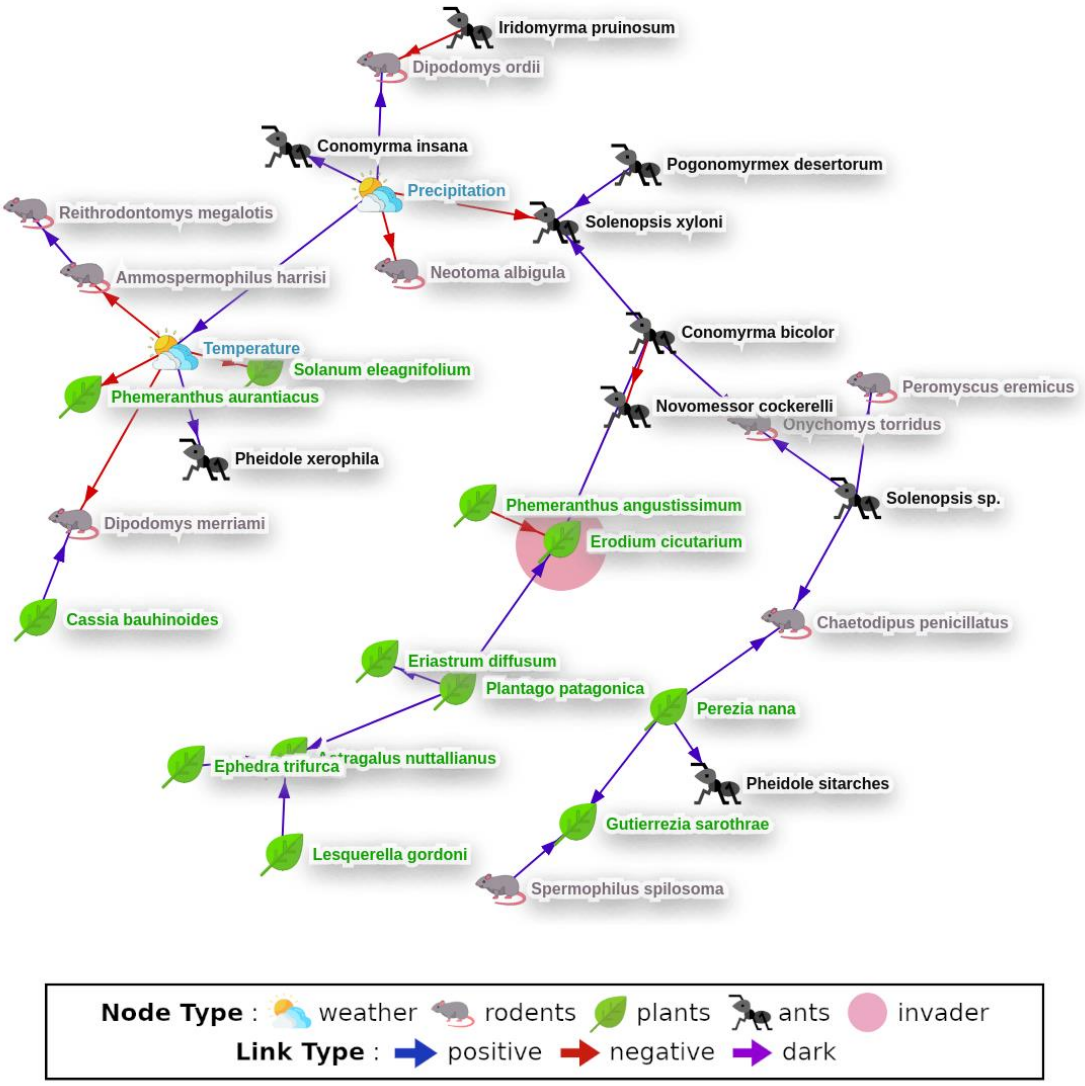

Figure S3. Aggregate causal network during the invasion period of Erodium cicutarium. The node icon is representative of the node's type (ants, plants, rodents, weather). The link color denotes type of causality (blue for positive, red for negative and purple for dark).

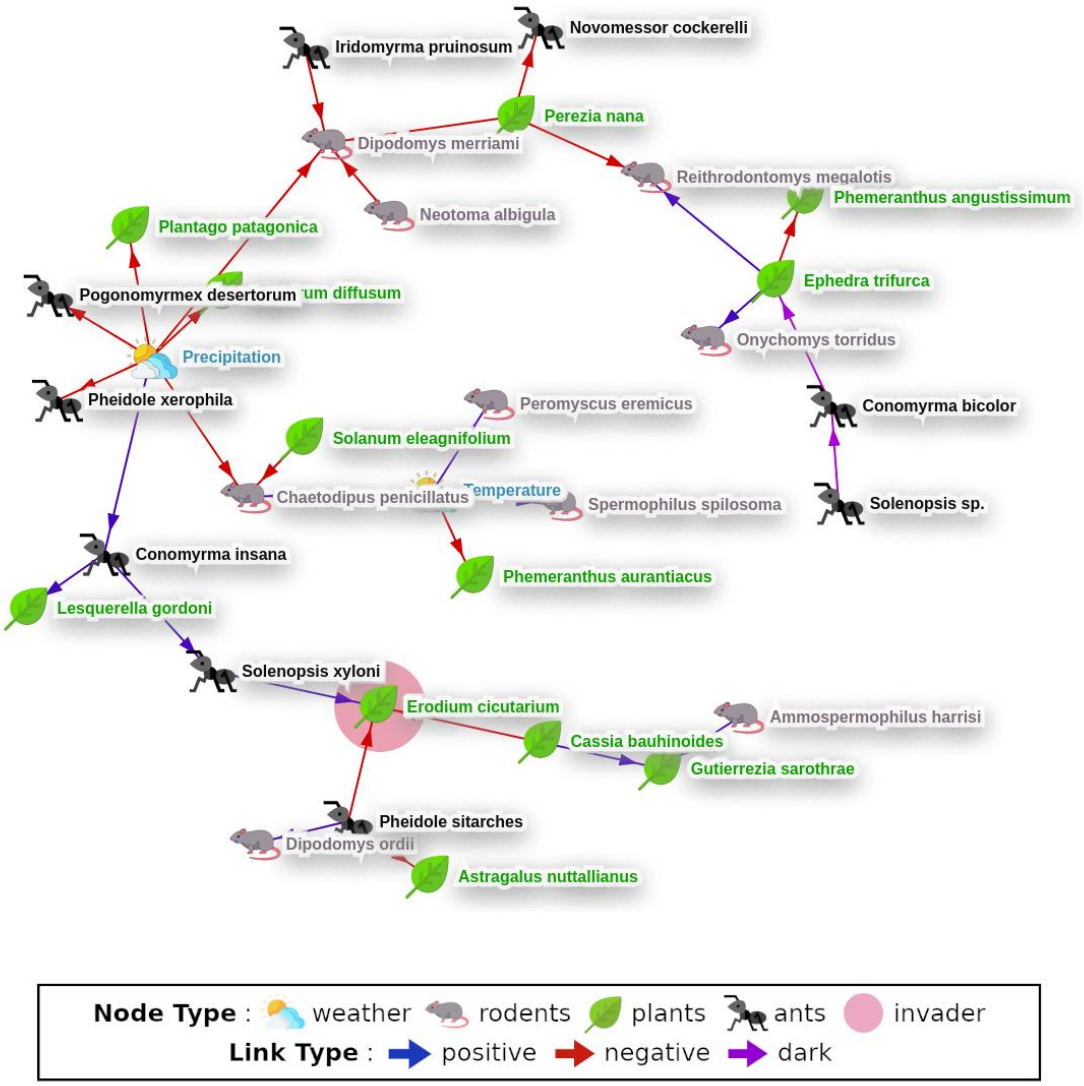

Figure S4. Aggregate causal network during the invasion period of Erodium cicutarium. The node icon is representative of the node's type (ants, plants, rodents, weather). The link color denotes type of causality (blue for positive, red for negative and purple for dark).

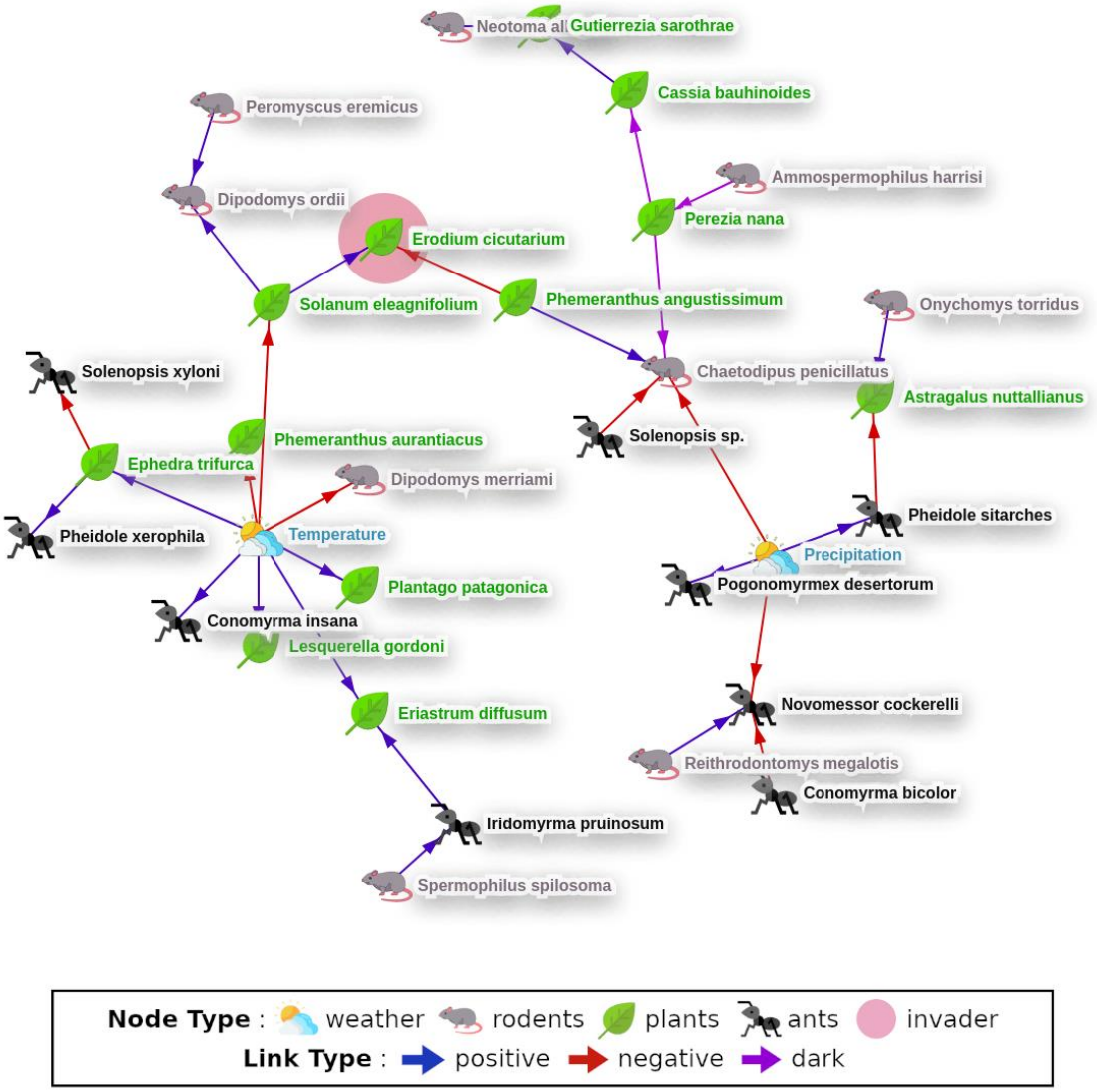

Figure S5. Aggregate causal network during the invasion period of Erodium cicutarium. The node icon is representative of the node's type (ants, plants, rodents, weather). The link color denotes type of causality (blue for positive, red for negative and purple for dark).

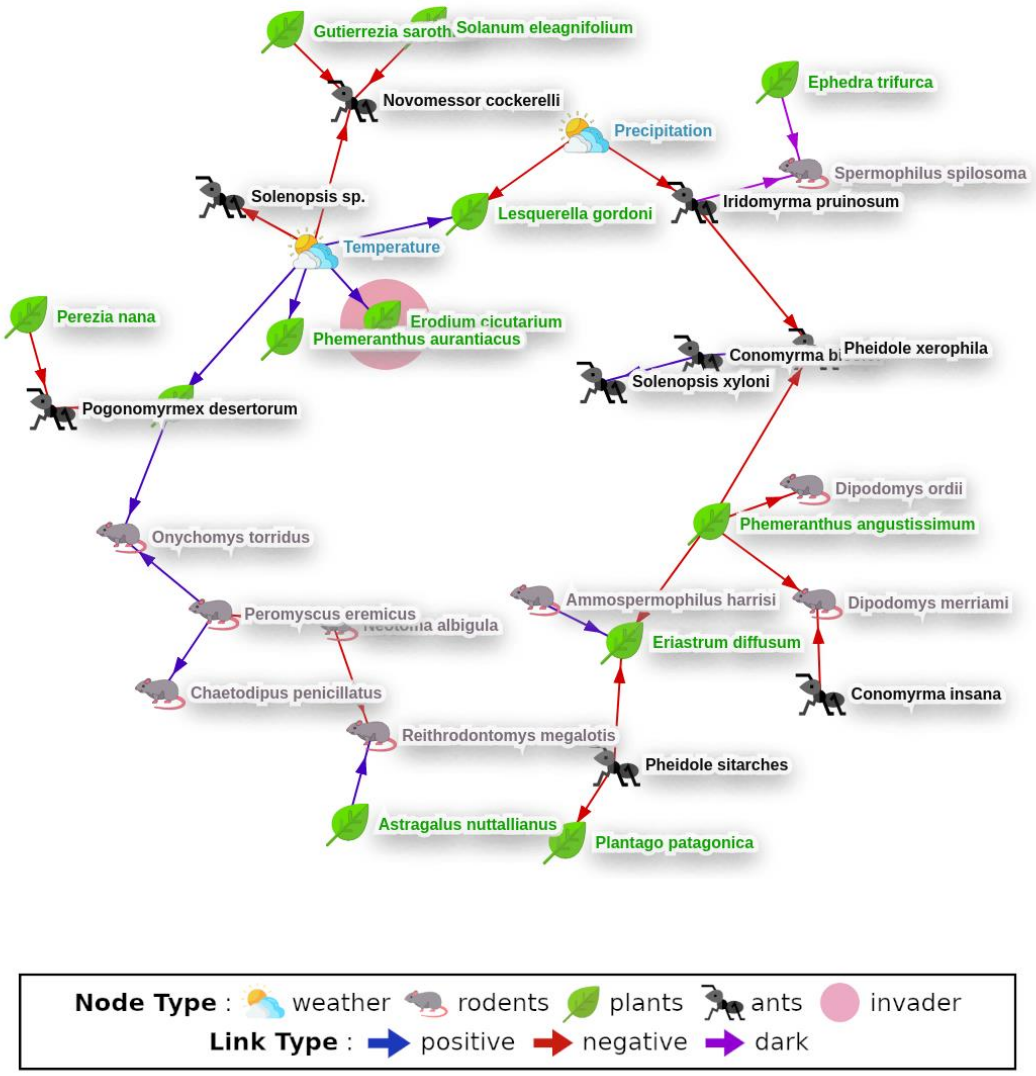

Figure S6. Aggregate causal network during the post-invasion period of Erodium cicutarium. The node icon is representative of the node's type (ants, plants, rodents, weather). The link color denotes type of causality (blue for positive, red for negative and purple for dark).

Details of the brain system

We use data of 20 subjects from a dataset made available publicly by Henri Begleiter of the Neurodynamics Laboratory of the State University of New York Health Center in Brooklyn, source: http://archive.ics.uci.edu/ml/datasets/EEG+Database. Each subject has undergone five trials and for each trial there are recordings in time series (L=256) from the 64 electrodes' voltage measurements. In order to have a panoramic comparison of EEG activity between the alcoholic and control subjects we adhered to a meticulous procedure. First, for each subject and for each trial, we calculated the underlying EEG network using the 64 electrodes as nodes and $E = 3, \tau = 1$ and $h = 1$ as parameters. At this point, we had 20×5×3=300 networks (three corresponding to the positive, negative and dark aspects). Then, for each subject, we created three resultant dynamic networks, averaging across the five trials. At this point, we had 20×3=60 averaged dynamic networks accounting for all 20 subjects. Finally, in order to compare the alcoholic versus control network structures, we averaged out the 10×3 networks for each type of subject (alcoholic and control). Thus, for our analysis, we kept three networks (positive, negative and dark) for the "average alcoholic" and three for the "average control" brain. When we refer to three networks, in fact, we are viewing the same network from three different aspects (positive, negative and dark), for the alcoholic and control subjects separately.

Table S3. List of all electrodes according to brain region.

Frontal region (1)	**Central region (2)**	**Parietal region (3)**	**Occipital region (4)**	**Temporal region (5)**	**Auxiliary electrodes (*)**
FP1	*FC1*	*CP1*	*PO1*	*T7*	*X*
FP2	*FC2*	*CP2*	*PO2*	*T8*	*Y*
FPZ	*FC3*	*CPZ*	*POZ*	*TP7*	*nd*
AF7	*FC4*	*CP3*	*PO7*	*TP8*	
AF8	*FC5*	*CP4*	*PO8*	*CP5*	
AF1	*FC6*	*PZ*	*O1*	*CP6*	
AF2	*FCZ*	*P1*	*O2*	*P7*	
AFZ	*CZ*	*P2*	*OZ*	*P8*	
F7	*C1*	*P3*		*P5*	
F8	*C2*	*P4*		*P6*	
F6	*C3*			*FT7*	
F3	*C4*			*FT8*	
F4	*C5*				
F1	*C6*				
F2					
FZ					
F5					

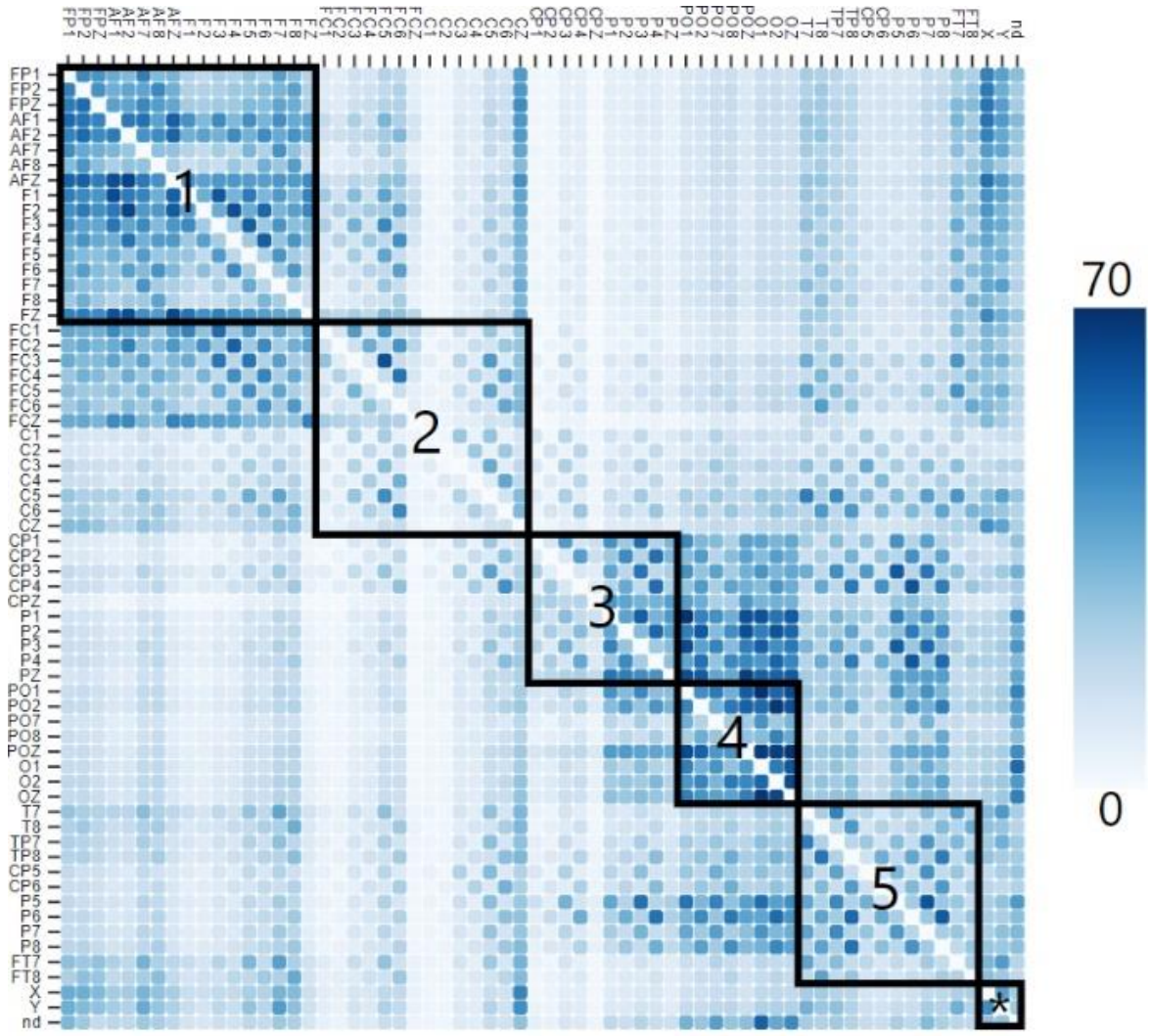

Alcoholic Brain (Positive)

Figure S7. Cumulative adjacency matrix for the average positive network structure of alcoholic brain. Box 1 corresponds to frontal region, box 2 corresponds to central region, box 3 corresponds to parietal region, box 4 corresponds to occipital region, box 5 corresponds to temporal region, and box * concerns auxiliary electrodes.

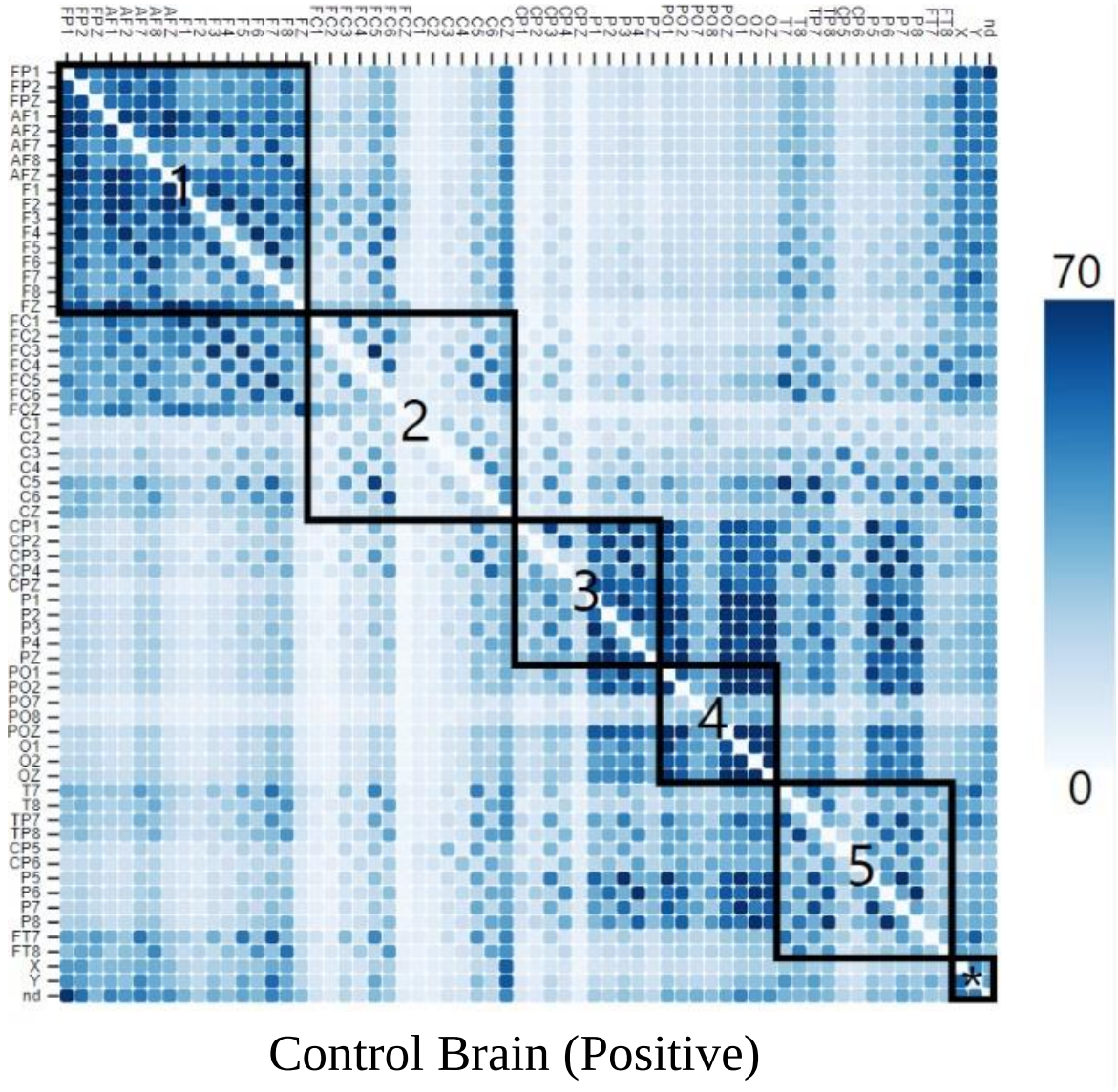

Figure S8. Cumulative adjacency matrix for the average positive network structure of control brain. Box 1 corresponds to frontal region, box 2 corresponds to central region, box 3 corresponds to parietal region, box 4 corresponds to occipital region, box 5 corresponds to temporal region, and box * concerns auxiliary electrodes.

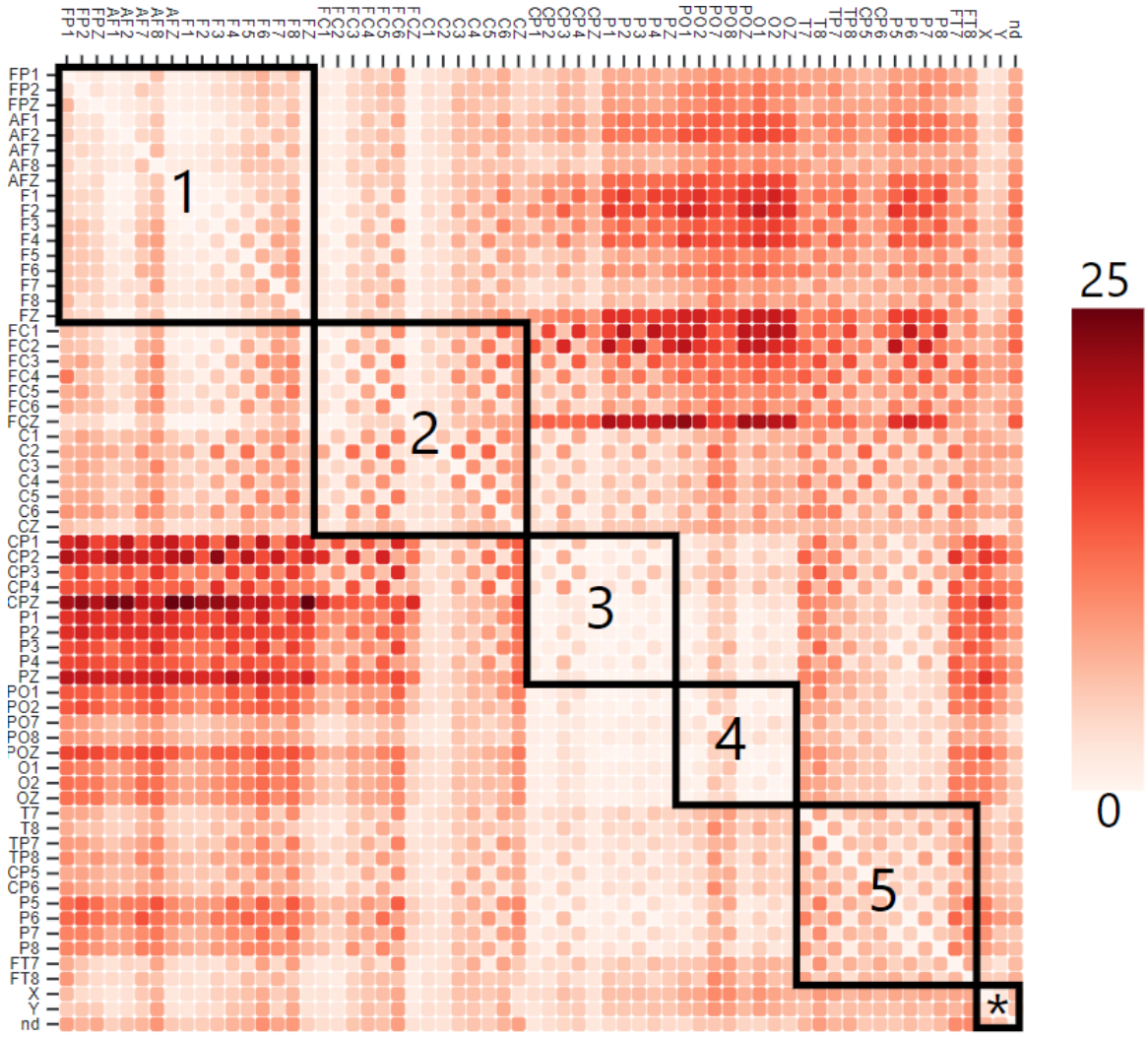

Figure S9. Cumulative adjacency matrix for the average negative network structure of alcoholic brain. Box 1 corresponds to frontal region, box 2 corresponds to central region, box 3 corresponds to parietal region, box 4 corresponds to occipital region, box 5 corresponds to temporal region, and box * concerns auxiliary electrodes.

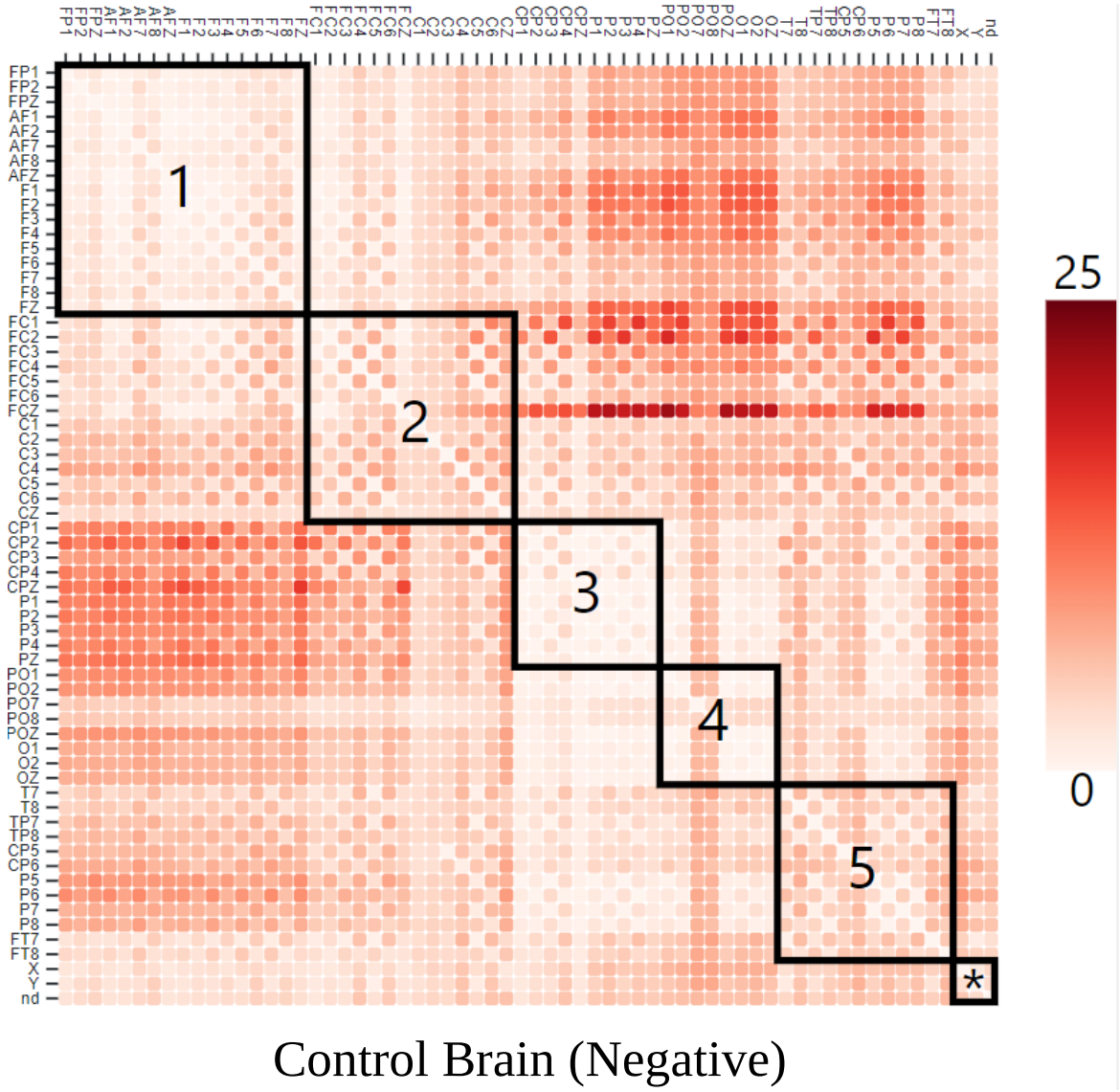

Figure S10. Cumulative adjacency matrix for the average negative network structure of control brain. Box 1 corresponds to frontal region, box 2 corresponds to central region, box 3 corresponds to parietal region, box 4 corresponds to occipital region, box 5 corresponds to temporal region, and box * concerns auxiliary electrodes.

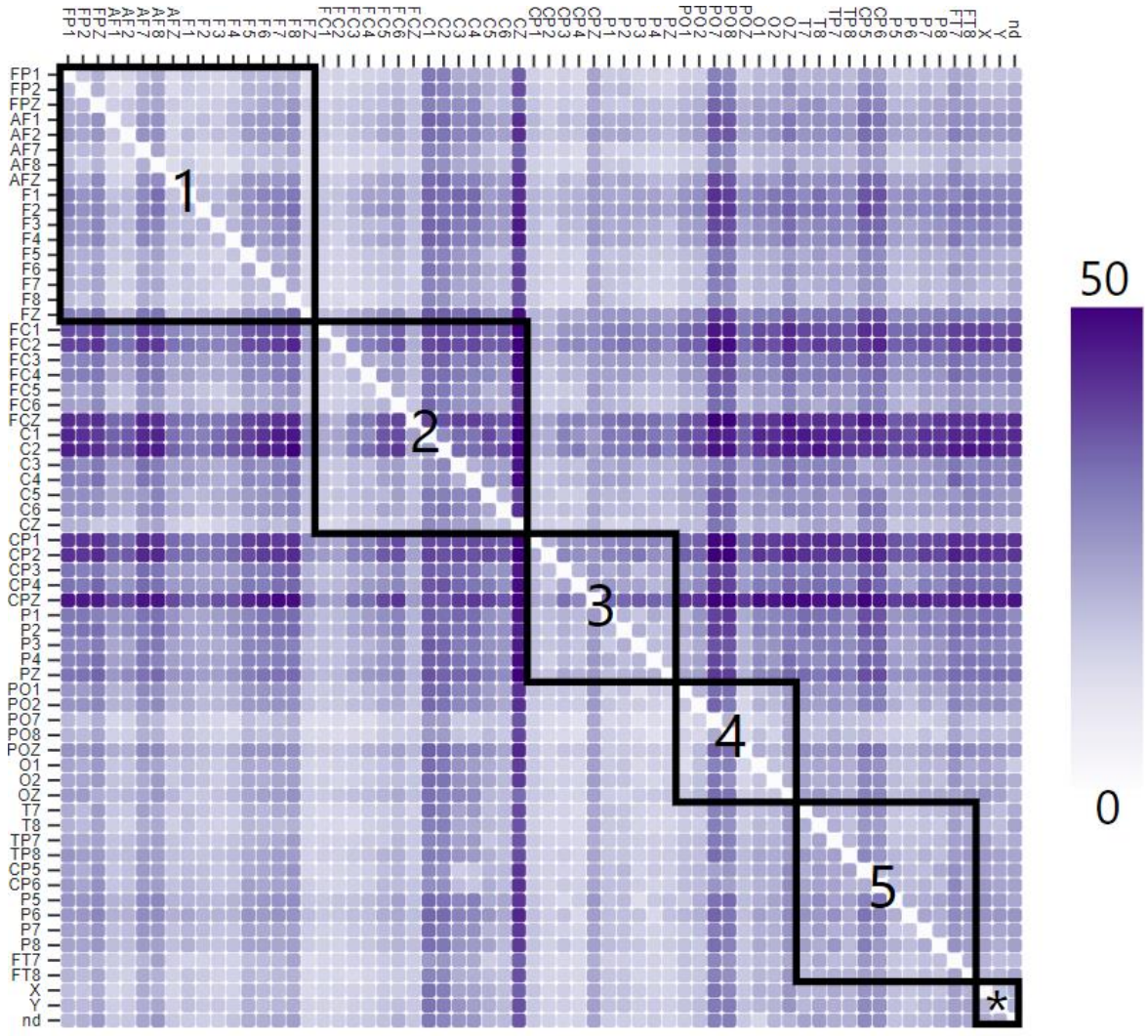

Alcoholic Brain (Dark)

Figure S11. Cumulative adjacency matrix for the average dark network structure of alcoholic brain. Box 1 corresponds to frontal region, box 2 corresponds to central region, box 3 corresponds to parietal region, box 4 corresponds to occipital region, box 5 corresponds to temporal region, and box * concerns auxiliary electrodes.

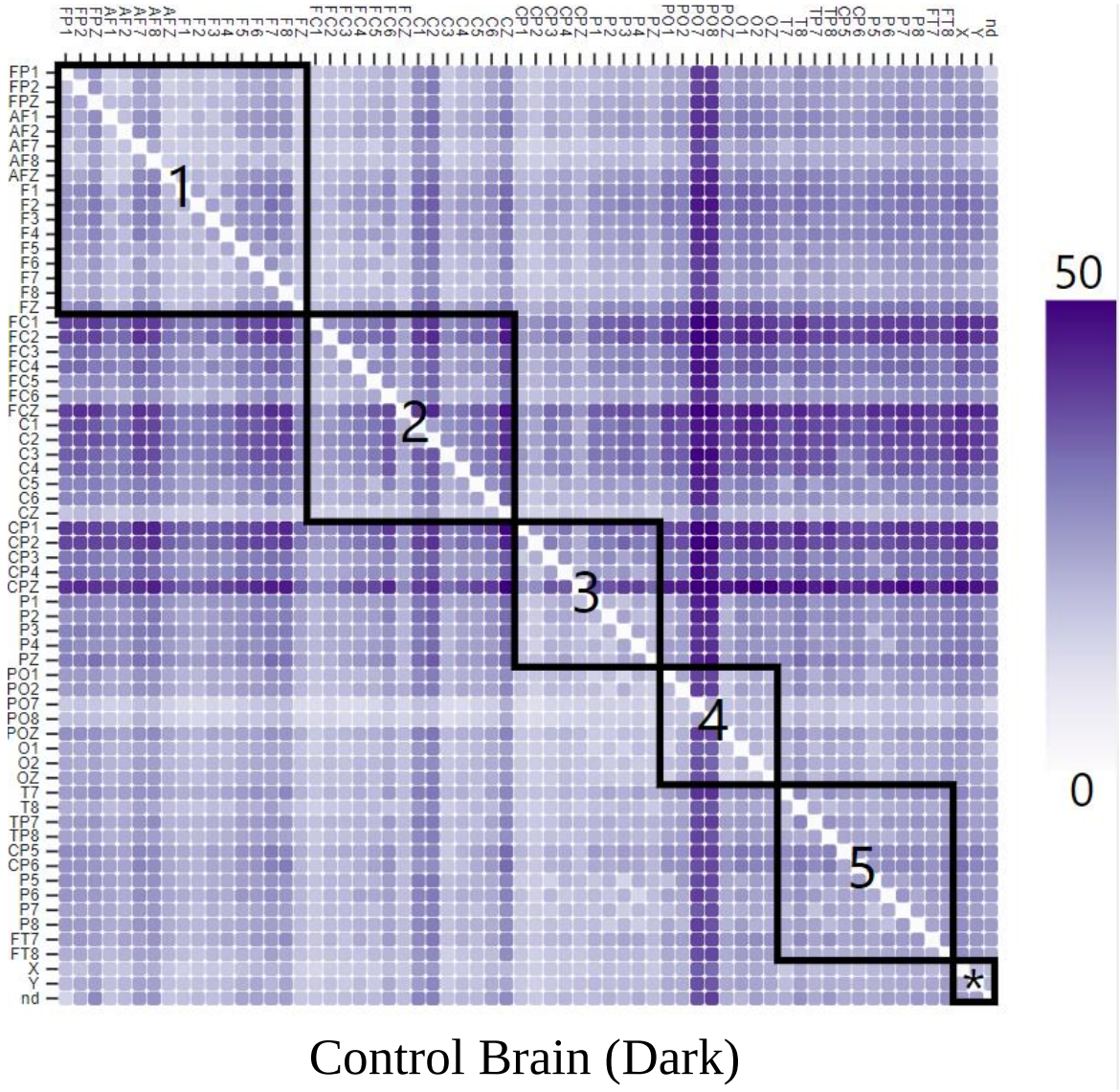

Figure S12. Cumulative adjacency matrix for the average dark network structure of control brain. Box 1 corresponds to frontal region, box 2 corresponds to central region, box 3 corresponds to parietal region, box 4 corresponds to occipital region, box 5 corresponds to temporal region, and box * concerns auxiliary electrodes.

Details of CDS network

Initially, we built a next-day-prediction network (day by day) from 2007 December 14 to 2019 May 13. To do this, we extracted the underlying interdependencies, with $E = 3, \tau = 1$ and $h = 1$. Thus, we could view the same network from three different spectra (positive, negative and dark). In Figures S13-S15, we present a cumulative adjacency matrix for each spectrum, where the color is associated with cumulative intensity. Darker colors denote stronger links overall.

Table S4. Senior prime banking Credit Default Swaps (CDS) of five-year maturity

1	Alliance & Leicester International Limited	35	Deutsche Bank AG
2	Allied Irish Banks	36	DNB ASA
3	Alpha Bank SA	37	Erste Group Bank AG
4	American Express Co	38	Fun Banc Caixa Dest
5	Australia and New Zealand Banking Group	39	Goldman Sachs Group
6	Banca Italease SPA	40	HSBC Bank PLC
7	Banca Monte Paschi	41	HSBC Holdings PLC
8	Banco Com Portugues	42	IKB Deutsche Industriebank AG
9	Banco De Sabadell	43	ING Bank N.V.
10	Banco Pop Espanol	44	Intesa Sanpaolo SPA
11	Banco Santander SA	45	Irish Bank Resolution Corp.
12	Bank of America	46	KBC Bank
13	Bank of Ireland	47	Landesbank Baden-Württemberg
14	Bank of Scotland	48	Macquarie Bank Ltd
15	Barclays Bank PLC	49	Mediobanca SPA
16	Barclays SLCSM Limited	50	National Bank of Greece SA
17	Bawag PSK	51	National Australian Bank
18	Bayerische Landesbank	52	Natixis
19	Banco Bilbao Vizcaya Argentaria SA	53	Natwest Markets PLC
20	Banca Nazionale Del Lavoro	54	Norddeutsche Landesbank
21	Bank of New York Mellon Corp.	55	Nordea Bank AB
22	Bank of America NA	56	Portigon AG
23	Banco Espírito Santo	57	Raif Zentralbank
24	BNP Paribas SA	58	Santander UK PLC
25	Capital One Bank USA NA	59	Skandinaviska Enskilda Banken
26	Capital One Financial	60	Societe Generale
27	CDA De Valencia Castellan	61	Standard Chartered Bank
28	CDA Y MP De Madrid	62	Skandinaviska Enskilda Banken
29	Citigroup Inc.	63	The PNC Financial Services Group
30	CMWL Bank Of Australia	64	The Royal Bank of Scotland Group plc
31	Commerzbank AG	65	UBS AG
32	Coop Rabobank UA	66	Unione Di Banche
33	Danske Bank A/S	67	Van Lanschot N.V.
34	De Volksbank NV	68	Westpac Banking Corp

Table S5. Top 10 most influential CDS of all time, ranked by subtracting cumulative in-strength centrality from out-strength centrality

Positive (Top 10 CDS)	**Negative (Top 10 CDS)**	**Dark (Top 10 CDS)**
Skandinaviska Enskilda Banken	Landesbank Baden-Württemberg	Santander UK PLC
Nordea Bank AB	Bawag PSK	IKB Dt Indstrbk AG
Skandinaviska Enskilda Banken	IKB Dt Indstrbk AG	Capital One Financial
Coop Rabobank UA	Norddeutsche Landesbank	Skandinaviska Enskilda Banken
Landesbank Baden-Württemberg	Alpha Bank SA	American Express Co
Danske Bank A/S	The PNC Financial Services Group	Capital One Bank USA NA
Bayerische Landesbk	National Bank Of Greece SA	Bawag PSK
HSBC Holdings PLC	Barclays SLCSM Ltd	Bayerische Landesbk
HSBC Bank PLC	Portigon AG	Cmwl Bk of Australia
Capital One Bank USA NA	Van Lanschot N.V.	Australia and New Zealand Banking Group

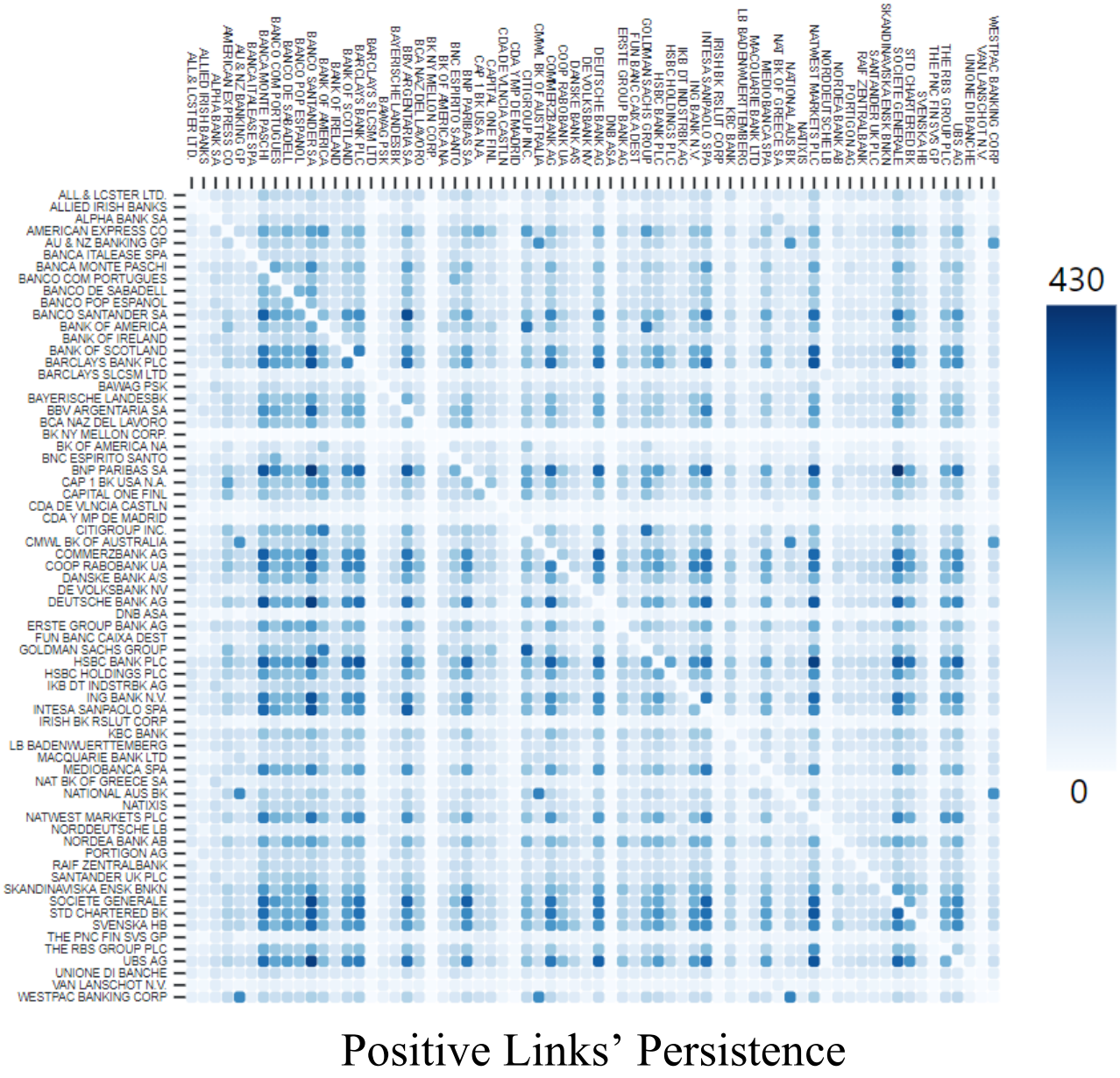

Figure S13. Cumulative Adjacency Matrix for the positive type of interdependencies on the last day of the time series data (2019 May 13). Darker color denotes higher accumulated link strength.

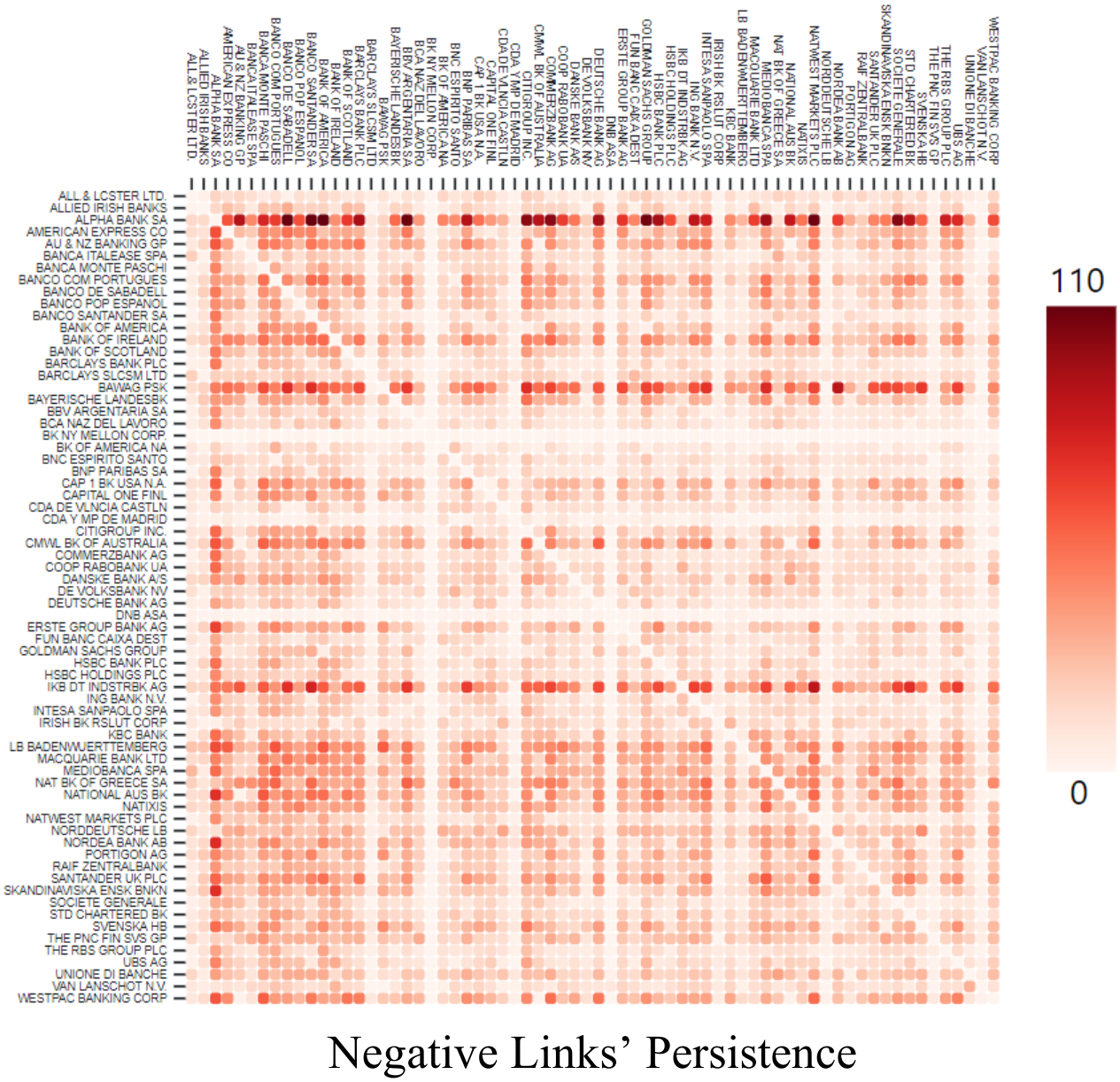

Figure S14. Cumulative Adjacency Matrix for the negative type of interdependencies on the last day of the time series data (2019 May 13). Darker color denotes higher accumulated link strength.

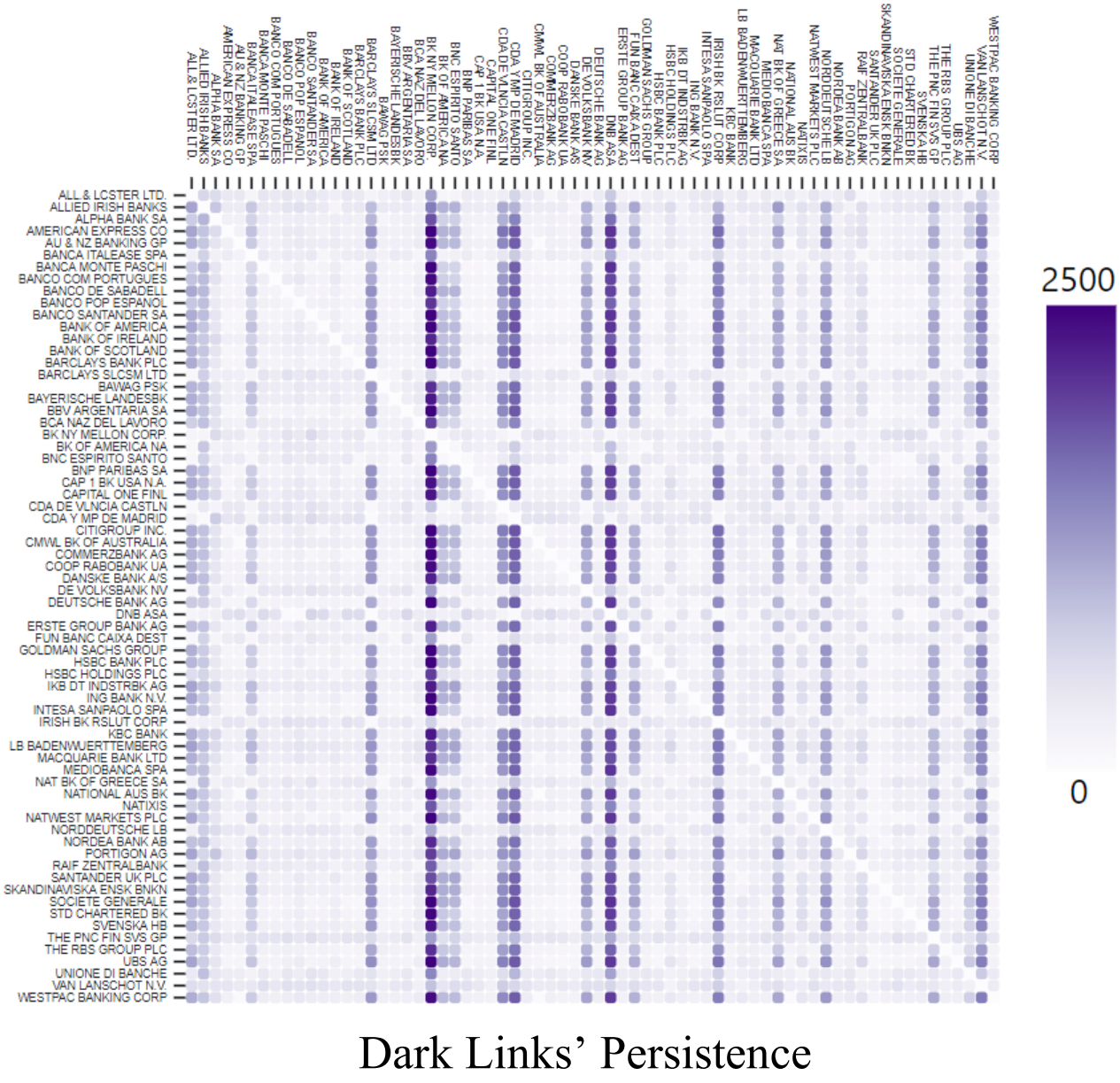

Dark Links' Persistence

Figure S15. Cumulative Adjacency Matrix for the dark type of interdependencies on the last day of the time series data (2019 May 13). Darker color denotes higher accumulated link strength.

6. From Time Series to Reconstructed Attractors

Dynamical systems theory states that the temporal evolution of a system is defined in some state space (or phase space, for continuous systems). The perception of the "state of a system" is powerful, even for nondeterministic systems. For example, stochastic Markov processes can be expressed through a set of states, along with a set of transition probabilities which define the random transition rules of the system. Specifying a point ω in this space $\mathbb{R}^m$ specifies the state of the system and vice versa. Thus, in this paper, in order to tap into the dynamics of the system, we employ the dynamics of the points in the corresponding state space, through an m-dimensional mapping. A sequence of points $\omega(t)$ is called a "trajectory" of the dynamical system, and $\omega(0)$ denotes the respective "initial conditions". For many dynamical systems, the trajectory will, after some time, be attracted to some subset of the state space. This set is invariant under the dynamical evolution, is called the "attractor" of the system, and can be studied as a manifold (Kantz & Schreiber 2004).

At their conception, time-series analysis and manifolds were two remotely distant areas of research, the first being on the very practical edge of statistics, and the second, antithetically, in the sphere of pure mathematics. A first promising result with the potential to bridge the two seemingly incompatible disciplines was Whitney's embedding theorem (1936), which suggests that a generic map from an *m*-dimensional manifold *M* to $\mathbb{R}^{2m+1}$ is an embedding, i.e. the image of *M* is completely unfolded in the higher-dimensional space. Notably, no two points in *M* map to the same point in $\mathbb{R}^{2m+1}$ (injective property). As $2m+1$ independent measurements (a time series) of a system can be considered a map from the set of states of *M* to $\mathbb{R}^{2m+1}$, Whitney's theorem suggests that each state can be identified uniquely by a vector of $2m+1$ time-series measurements, thereby reconstructing the state space. However, practically speaking, most scientists end up with some time series without any awareness of the overall state space and its dimension m. Moreover, even if they did know the value of m, according to Whitney, they would need $2m+1$ distinct time series to be able to reconstruct the original state space. Due to the apparent impracticality for experimental settings, Whitney's theorem, despite being

monumental for differential topology, did not ignite a connection between time series and manifolds.

Half a century later, Takens' (1981) embedding theorem, along with a first practical study (Packard et al., 1980), bridged the gap, and a burgeoning literature of time-series methods capitalized on the newly unlocked insights from differentiable manifolds. The contribution of Takens' theorem was to show that state space reconstruction could be achieved with just a single time series. Takens proved that, instead of $2m + 1$ distinct time series, the time-delayed versions $[X(t), X(t-\tau), X(t-2\tau), \dots, X(t-2m\tau)]$ of one time series X would suffice to embed the m-dimensional manifold. Moreover, Takens showed that reconstruction is viable even in a space with dimension $E \leq 2m + 1$. This theorem liberated the attractor reconstruction task from the need to find $2m + 1$ distinct time series and enabled every single time series to be analyzed in its time-delayed form, provided that m could somehow be approached. A decade later, Sauer et al. (1991) were able to generalize both Whitney's and Takens' theorems to fractal dimensions as well.

Therefore, practically speaking, in order to study the hidden dynamics of a time series, one needs to embed it in a dimension E using a lag τ. In order to retrieve the optimal combination of E and τ, there are various methods in the literature (Fraser & Swinney 1986; Farmer & Sidorowich 1987; Casdagli 1989; Liebert & Schuster 1989; Kennel et al. 1992; Cellucci et al. 2003; Krakovska et al. 2015). Nevertheless, with today's computational power, optimal pairs of E and τ can be found by trial and error, comparing the results in terms of forecasting accuracy for a whole range of reasonable embedding parameters (E, τ).

7. Theorems and Proofs

Let X, Y be any two variables evolving through time which belong to a common dynamical system. Their trajectories $X(t)$ and $Y(t)$ are attracted over time to the m-dimensional attractor manifold M of the system. Let the time lags of $X(t)$ and $Y(t)$ be embedded into a state space with dimension E and, using delay τ, let them create E-dimensional trajectories of vectors $\underline{x}(t) =< X(t), X(t-\tau), \dots, X(t-(E-1)\tau) >$ and $\underline{y}(t) =< Y(t), Y(t-\tau), \dots, Y(t-(E-1)\tau) >$ respectively. The sets of all points $\underline{x}(t)$ and $\underline{y}(t)$ are known as

reconstructed attractor manifolds or shadow attractors and are notated as M_X and M_Y respectively. Since causality (statistical influence) is the quantifiable influence exerted by one variable X on another variable Y, unlike correlation which distinguishes between positive and negative relations in time-series analysis, the other measures of statistical influence tend to ignore the nature of interactions (for more discussion, see Stavroglou et al. 2019). Therefore, as a next step, an important definition is provided, which enables identification of the nature of influence.

Definition 1.

1) If X causes same-direction changes to Y, then we say that X has a positive influence on Y.
2) If X causes opposite-direction changes to Y, then we say that X has a negative influence on Y.
3) If X causes changes to Y which are of neither the same nor the opposite direction, then we say that X has a "dark" influence on Y.
4) $\twoheadrightarrow$ symbolizes diffeomorphism.

The following results provide the mathematical setting needed for deducing influence in a dynamical systems framework. In what follows, by smooth functions, we mean at least $\mathbb{C}^2$ (the derivatives of up to order 2 exist and are continuous).

Lemma 1. *Let M be an m-dimensional compact manifold and $X: M \to \mathbb{R}$, $Y: M \to \mathbb{R}$ be smooth observation functions. Let $\varphi: M \twoheadrightarrow M$ be a smooth diffeomorphism. If there exists $\psi: M_X \twoheadrightarrow M_Y$ such that ψ is bijective, then M_X causes M_Y.*

Proof of Lemma 1: Since X, Y are smooth functions and φ is a smooth diffeomorphism, according to Takens' theorem it is a generic property that the maps $\Phi_{(\varphi,X)}(\underline{\omega}): M \to \mathbb{R}^{2m+1}$ and $\Phi_{(\varphi,Y)}(\underline{\omega}): M \to \mathbb{R}^{2m+1}$, defined as

$$\Phi_{(\varphi,X)}(\underline{\omega}) = \langle X(\underline{\omega}), X(\varphi(\underline{\omega})), \dots, X(\varphi^{2m}(\underline{\omega})) \rangle$$

$$\Phi_{(\varphi,Y)}(\underline{\omega}) = \langle Y(\underline{\omega}), Y(\varphi(\underline{\omega})), \dots, Y(\varphi^{2m}(\underline{\omega})) \rangle$$

are embeddings (reconstructions) of the original manifold M and $\underline{\omega} \in M$.

Specifically, $M_X: \{\underline{x} = \Phi_{(\varphi,X)}(\underline{\omega}) | \underline{\omega} \in M\}$ and $M_Y: \left\{\underline{y} = \Phi_{(\varphi,Y)}(\underline{\omega}) \middle| \underline{\omega} \in M\right\}$.

Since $\exists\, \psi: M_X \rightarrowtail\!\!\!\!\!\rightarrow M_Y$, with ψ bijective (injective and surjective), this means

1) $\forall \underline{x}, \underline{x}' \in M_X,\ \psi(\underline{x}) = \psi(\underline{x}') \Longrightarrow \underline{x} = \underline{x}'$, or equivalently $\forall \underline{x}, \underline{x}' \in M_X,\ \underline{x} \neq \underline{x}' \Longrightarrow \psi(\underline{x}) \neq \psi(\underline{x}')$, and
2) $\forall \underline{y} \in M_Y, \exists!\ \underline{x} \in M_X, \psi(\underline{x}) = \underline{y}$

From (2), it is obvious that, since every point $\underline{y}$ in M_Y is determined via ψ from a unique point $\underline{x}$ from M_X, M_X causes M_Y in line with Definition 1. ■

The following lemma provides the necessary ingredients for us to logically deduce influence from shadow attractors on their respective time series.

Lemma 2. *Let M be an m-dimensional compact manifold and $X: M \to \mathbb{R}$, $Y: M \to \mathbb{R}$ be smooth observation functions. If M_X causes M_Y (through a bijective map ψ) and there exist $h: M_X \rightarrowtail\!\!\!\!\!\rightarrow X$ and $g: M_Y \rightarrowtail\!\!\!\!\!\rightarrow Y$, with h, g bijective, then X causes Y as well.*

Proof of Lemma 2: According to Lemma 1, since M_X causes M_Y, there exists a bijective map ψ such that $\forall \underline{y} \in M_Y, \exists!\ \underline{x} \in M_X, \psi(\underline{x}) = \underline{y}$.

Since h, g are bijective, $\forall \underline{x} \in M_X, \exists!\ x \in X, \mathrm{h}(\underline{x}) = x$, and $\forall \underline{y} \in M_Y, \exists!\ y \in Y, \mathrm{g}\left(\underline{y}\right) = y$.

Thus,

$\psi(\underline{x}) = \underline{y} \Leftrightarrow \psi(\,\mathrm{h}(x)) = \mathrm{g}(y) \overset{g^{-1}:bijective}{\Longleftrightarrow} (g^{-1} \circ \psi \circ h)(x) = (g^{-1} \circ g)(y) \Leftrightarrow y = (g^{-1} \circ \psi \circ h)(x)$.

By setting $(g^{-1} \circ \psi \circ h) = \rho, y = \rho(x), \forall y \in Y$.

From the last equation, it is obvious that, since every y in Y is determined via ρ from a unique point x from X, X causes Y, in line with Definition 1. ■

Remark: The composition of bijective functions is a bijection.

As articulated in Lemmas 1 and 2, strong influence from X to Y is established by X having an influence on all values of Y. This is achieved primarily through the bijective property firstly of $\psi: M_X \rightarrowtail\!\!\!\!\!\rightarrow M_Y$ and subsequently of $h: M_X \rightarrowtail\!\!\!\!\!\rightarrow X$ and $g: M_Y \rightarrowtail\!\!\!\!\!\rightarrow Y$. Bijection

guarantees that, ultimately, at every time step of the dynamical evolution, *Y* is influenced by *X*, thus *X* strongly causes *Y*. The following two lemmas are similar to Lemmas 1 and 2, with the only difference being that we relax the requirement for a bijective mapping to an injective mappying, and thus the deduction is "weak" influence. This form of influence is what we expect to find in real data.

Lemma 3. *Let M be an m-dimensional compact manifold and $X: M \to \mathbb{R}$, $Y: M \to \mathbb{R}$ be smooth observation functions. Let $\varphi: M \twoheadrightarrow M$ be a smooth diffeomorphism. If there exists $\psi: M_X \rightarrowtail M_Y$ such that ψ is injective, then M_X weakly causes M_Y.*

Proof of Lemma 3: Since *X*, *Y* are smooth functions and φ is a smooth diffeomorphism, according to Takens' theorem, it is a generic property that the maps $\Phi_{(\varphi,X)}(\underline{\omega}): M \to \mathbb{R}^{2m+1}$ and $\Phi_{(\varphi,Y)}(\underline{\omega}): M \to \mathbb{R}^{2m+1}$, defined as

$$\Phi_{(\varphi,X)}(\underline{\omega}) = \langle X(\underline{\omega}), X(\varphi(\underline{\omega})), \dots, X(\varphi^{2m}(\underline{\omega})) \rangle$$

$$\Phi_{(\varphi,Y)}(\underline{\omega}) = \langle Y(\underline{\omega}), Y(\varphi(\underline{\omega})), \dots, Y(\varphi^{2m}(\underline{\omega})) \rangle$$

are embeddings (reconstructions) of the original manifold M and $\underline{\omega} \in M$.

Specifically, $M_X: \{\underline{x} = \Phi_{(\varphi,X)}(\underline{\omega}) | \underline{\omega} \in M\}$ and $M_Y: \{\underline{y} = \Phi_{(\varphi,Y)}(\underline{\omega}) | \underline{\omega} \in M\}$.

Since $\exists\, \psi: M_X \rightarrowtail M_Y$, with ψ being injective, this means

1) $\forall \underline{x}, \underline{x}' \in M_X,\ \psi(\underline{x}) = \psi(\underline{x}') \Longrightarrow \underline{x} = \underline{x}'$, or equivalently, $\forall \underline{x}, \underline{x}' \in M_X,\ \underline{x} \neq \underline{x}' \Longrightarrow \psi(\underline{x}) \neq \psi(\underline{x}')$, and
2) $\forall \underline{y} \in M_Y,\ \exists_{\leq 1}\, \underline{x} \in M_X, \psi(\underline{x}) = \underline{y}$

From (2), it is obvious that every point $\underline{y}$ in M_Y is determined by at most one $\underline{x} \in M_X$ (it is not guaranteed, though, that every $\underline{y}$ is determined by some $\underline{x}$, thus the influence is "weak", unlike with a bijective ψ). Thus M_X causes M_Y, in line with Definition 1. ■

Lemma 4. *Let M be an m-dimensional compact manifold and $X: M \to \mathbb{R}$, $Y: M \to \mathbb{R}$ be smooth observation functions. If M_X weakly causes M_Y (through an injective map ψ) and there exist $h: M_X \rightarrowtail X$ and $g: M_Y \rightarrowtail Y$ with h, g being injective, then X weakly causes Y as well.*

Proof of Lemma 4: According to Lemma 3, since M_X causes M_Y, there exists an injective map ψ such that $\forall \underline{y} \in M_Y,\ \exists_{\leq 1}\ \underline{x} \in M_X, \psi(\underline{x}) = \underline{y}$.

Since h, g are injective, $\forall \underline{x} \in M_X,\ \exists_{\leq 1}\ x \in X, \mathrm{h}(\underline{x}) = x,$ and $\forall \underline{y} \in M_Y,\ \exists_{\leq 1}\ y \in Y, \mathrm{g}(\underline{y}) = y.$

Thus,

$\psi(\underline{x}) = \underline{y} \Leftrightarrow \psi(\ \mathrm{h}(x)) = \mathrm{g}(y) \overset{g^{-1}:injective}{\Longleftrightarrow} (g^{-1} \circ \psi \circ h)(x) = (g^{-1} \circ g)(y) \Leftrightarrow y = (g^{-1} \circ \psi \circ h)(x).$

By setting $(g^{-1} \circ \psi \circ h) = \rho, y = \rho(x), \text{for some } y \in Y.$

From the last equation, it is obvious that some y in Y are determined via ρ from a unique point x from *X*. Thus, *X* causes *Y*, in line with Definition 1. ■

Remark: The composition of injective functions is an injection.

By relaxing the requirement from a bijection (see Lemmas 1 and 2) to an injection (see Lemmas 3 and 4), we expect that, for *X* to weakly cause *Y*, essentially, ψ, *h* and *g* have to be injective. Injection suggests that, at some time steps of the dynamical evolution, *Y* is influenced by *X*, thus *X* weakly causes *Y*, and the strength of influence is determined by the frequency of the mapping. Having established the prerequisite lemmas, we are now in a position to develop the main results that allow the nature of influence to be expressed and quantified. To that end, we need to use patterns from symbolic dynamics theory (see Section 2: Determining the nature of influence).

Now filtering the vectors $\underline{x}(t) \in M_X$ and $\underline{y}(t) \in M_Y$ through symbolic dynamics, we can extract their corresponding patterns $P_{\underline{x}(t)}$ and $P_{\underline{y}(t)}$ and we can distinguish three types of mappings (see Tables S7 and S8 in Section 8).

Definition 2.

i) $\mathcal{P}: M_X \overset{+}{\rightarrow} M_Y,\ \overset{+}{\rightarrow}: \{\underline{x} \rightarrow \underline{y} | P_{\underline{x}} \overset{+}{\leftrightarrow} P_{\underline{x}}\}$, $\mathcal{P}$ corresponds to the same patterns (i.e. positive mapping)

ii) $\mathcal{N}: M_X \overset{-}{\rightarrow} M_Y$, $\overset{-}{\rightarrow}: \{\underline{x} \rightarrow \underline{y} | P_{\underline{x}} \overset{-}{\leftrightarrow} P_{\underline{x}}\}$, $\mathcal{N}$ corresponds to opposite patterns (i.e. negative mapping)

iii) $\mathcal{D}: M_X \overset{\star}{\rightarrow} M_Y$, $\overset{\star}{\rightarrow}: \{\underline{x} \rightarrow \underline{y} | P_{\underline{x}} \overset{\star}{\leftrightarrow} P_{\underline{x}}\}$, $\mathcal{D}$ corresponds to patterns that are neither the same nor opposite (i.e. dark mapping)

Definition 2 is used extensively in the formulation and proof of the following three important theorems.

Theorem 1. *Let M be an m-dimensional compact manifold and $X: M \rightarrow \mathbb{R}$, $Y: M \rightarrow \mathbb{R}$ be smooth observation functions. Let $\varphi: M \rightarrowtail M$ be a smooth diffeomorphism. Let M_X and M_Y be the shadow attractors of X and Y respectively. If $\mathcal{P}: M_X \overset{+}{\rightarrow} M_Y$ such that $\mathcal{P}$ is bijective (or injective) and there exist $h: M_X \rightarrow X$ and $g: M_Y \rightarrow Y$, with h, g being bijective (or injective), then X exerts a positive influence on Y.*

Proof of Theorem 1: Since X, Y are smooth functions and φ is a smooth diffeomorphism, according to Takens' theorem it is a generic property that the maps $\Phi_{(\varphi,X)}(\underline{\omega}): M \rightarrow \mathbb{R}^{2m+1}$ and $\Phi_{(\varphi,Y)}(\underline{\omega}): M \rightarrow \mathbb{R}^{2m+1}$are embeddings (reconstructions) of the original manifold M and $\underline{\omega} \in M$. Since $\exists\, \mathcal{P}: M_X \overset{+}{\rightarrow} M_Y$, with $\mathcal{P}$ being bijective (injective), according to Lemma 1 (or similarly Lemma 3), M_X causes M_Y, and since $\exists h, g$ that are bijective (injective), i.e., $h: M_X \rightarrow X$ and $g: M_Y \rightarrow Y$, according to Lemma 2 (or similarly Lemma 4), X causes Y. Since $\mathcal{P}$ refers only to same-pattern couplings, according to Definition 1, X exerts a positive influence on Y. ■

Theorem 2. *Let M be an m-dimensional compact manifold and $X: M \rightarrow \mathbb{R}$, $Y: M \rightarrow \mathbb{R}$ be smooth observation functions. Let $\varphi: M \rightarrowtail M$ be a smooth diffeomorphism. Let M_X and M_Y be the shadow attractors of X and Y respectively. If $\mathcal{N}: M_X \overset{-}{\rightarrow} M_Y$ is bijective (or injective) and there exist $h: M_X \rightarrow X$ and $g: M_Y \rightarrow Y$ that are bijective (or injective), then X exerts a negative influence on Y.*

Proof of Theorem 2: Since X, Y are smooth functions and φ is a smooth diffeomorphism, according to Takens' theorem, it is a generic property that the maps $\Phi_{(\varphi,X)}(\underline{\omega}): M \rightarrow \mathbb{R}^{2m+1}$ and $\Phi_{(\varphi,Y)}(\underline{\omega}): M \rightarrow \mathbb{R}^{2m+1}$are embeddings (reconstructions) of the original

manifold M and $\underline{\omega} \in M$. Since $\exists\, \mathcal{N}: M_X \xrightarrow{-} M_Y$, with $\mathcal{N}$ being bijective (injective), according to Lemma 1 (or similarly Lemma 3), M_X causes M_Y, and since $\exists h, g$ that are bijective (injective), i.e., $h: M_X \to X$ and $g: M_Y \to Y$, according to Lemma 2 (or similarly Lemma 4), X causes Y. Since $\mathcal{N}$ refers only to opposite-pattern couplings, according to Definition 1, X exerts a negative influence on Y. ■

Theorem 3. *Let M be an m-dimensional compact manifold and $X: M \to \mathbb{R}$, $Y: M \to \mathbb{R}$ be smooth observation functions. Let $\varphi: M \twoheadrightarrow M$ be a smooth diffeomorphism. Let M_X and M_Y be the shadow attractors of X and Y respectively. If $\mathcal{D}: M_X \xrightarrow{\star} M_Y$ such that $\mathcal{D}$ is bijective (or injective) and there exist $h: M_X \to X$ and $g: M_Y \to Y$, with h, g being bijective (or injective), then X exerts a dark influence on Y.*

Proof of Theorem 3: Since X, Y are smooth functions and φ is a smooth diffeomorphism, according to Takens' theorem, it is a generic property that the maps $\Phi_{(\varphi,X)}(\underline{\omega}): M \to \mathbb{R}^{2m+1}$ and $\Phi_{(\varphi,Y)}(\underline{\omega}): M \to \mathbb{R}^{2m+1}$are embeddings (reconstructions) of the original manifold M and $\underline{\omega} \in M$. Since $\exists\, \mathcal{D}: M_X \xrightarrow{\star} M_Y$, with $\mathcal{D}$ being bijective (injective), according to Lemma 1 (or similarly Lemma 3), M_X causes M_Y, and since $\exists h, g$ that are bijective (injective), i.e., $h: M_X \to X$ and $g: M_Y \to Y$, according to Lemma 2 (or similarly Lemma 4), X causes Y. Since $\mathcal{D}$ refers only to pattern couplings which are neither the same nor opposite, according to Definition 1, X exerts a dark influence on Y. ■

8. Signature Calculation and Pattern Causality Matrix

Let us have four patterns:

- $s_1 = \nearrow\nearrow = (0.32, 0.45)$, with corresponding weight, $w_1 = 0.91$.
- $s_2 = \searrow\nearrow = (-0.11, 0.51)$, with corresponding weight, $w_2 = 0.54$.
- $s_3 = \nearrow\nearrow = (0.13, 0.19)$, with corresponding weight, $w_3 = 0.82$.
- $s_4 = \nearrow\searrow = (0.05, -0.08)$, with corresponding weight, $w_4 = 0.69$.

The weighted average in our example is

$S = \sum_{i=1}^{4} w_i\, s_i = 0.91 * (0.32, 0.45) + 0.54 * (-0.11, 0.51) + 0.82 * (0.13, 0.19) +$
$0.69 * (0.05, -0.08) = (0.3729, 0.7855) = (\nearrow\nearrow)$

Thus, the emergent weighted average pattern is the signature of S: $\boldsymbol{P}$=$signature(S)$=$\nearrow\nearrow$.

Table S6. PC (from *X* to *Y*) pattern to pattern matrix for $E = 2$. Each cell is filled with the accuracy from step 6 of our algorithm. Thus, each cell takes values from 0 to 1. Blue cells denote positive influence. Red cells denote negative influence. Purple cells denote dark influence.

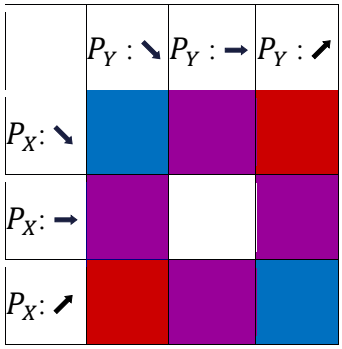

Table S7. PC (from *X* to *Y*) pattern to pattern matrix for $E = 3$. Each cell is filled with the accuracy from step 6 of our algorithm. Thus, each cell takes values from 0 to 1. Blue cells denote positive influence. Red cells denote negative influence. Purple cells denote dark influence.

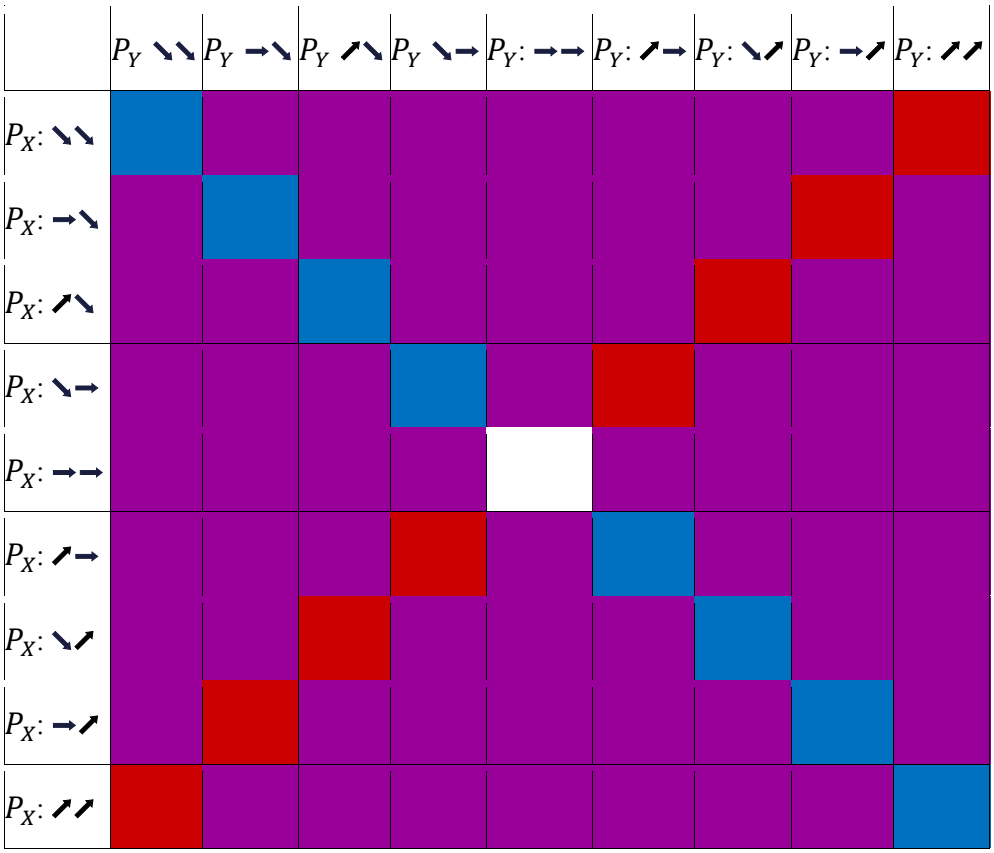

References

Barnes, J. A., & Harary, F. (1983). Graph theory in network analysis. Social Networks, **5**(2), 235-244.

DOI: https://doi.org/10.1016/0378-8733(83)90026-6

Barrat, A., Barthelemy, M., Pastor-Satorras, R., & Vespignani, A. (2004). The architecture of complex weighted networks. Proceedings of the National Academy of Sciences of U.S.A., **101**(11), 3747-3752.

DOI: https://doi.org/10.1073/pnas.0400087101

Bavelas, A. (1950). Communication patterns in task-oriented groups. The Journal of the Acoustical Society of America, **22**(6), 725-730.

DOI: https://doi.org/10.1121/1.1906679

Casdagli, M. (1989). Nonlinear prediction of chaotic time series. Physica D: Nonlinear Phenomena, **35**(3), 335-356.

DOI: https://doi.org/10.1016/0167-2789(89)90074-2

Cellucci, C. J., Albano, A. M., & Rapp, P. E. (2003). Comparative study of embedding methods. Physical Review E, **67**(6), 066210.

DOI: https://doi.org/10.1103/PhysRevE.67.066210

Coleman, T. F., & Moré, J. J. (1983). Estimation of sparse Jacobian matrices and graph coloring blems. SIAM Journal on Numerical Analysis, **20**(1), 187-209.

DOI: https://doi.org/10.1137/0720013

Eagle, N., Macy, M., & Claxton, R. (2010). Network diversity and economic development. Science, **328**(5981), 1029-1031.

DOI: https://doi.org/10.1126/science.1186605

Farmer, J. D., & Sidorowich, J. J. (1987). Predicting chaotic time series. Physical Review Letters, **59**(8), 845.

DOI: https://doi.org/10.1103/PhysRevLett.59.845

Fraser, A. M., & Swinney, H. L. (1986). Independent coordinates for strange attractors from mutual information. Physical Review A, **33**(2), 1134.

DOI: https://doi.org/10.1103/PhysRevA.33.1134

Freeman, L. C. (1977). A set of measures of centrality based on betweenness. Sociometry, 35-41.

DOI: http://dx.doi.org/10.2307/3033543

Freeman, L. C. (1978). Centrality in social networks conceptual clarification. Social Networks, **1**(3), 215-239.

DOI: http://dx.doi.org/ 10.1.1.227.9549

Hakimi, S. L. (1962). On realizability of a set of integers as degrees of the vertices of a linear graph. I. Journal of the Society for Industrial and Applied Mathematics, **10**(3), 496-506.

DOI: https://doi.org/10.1137/0111010

Hopcroft, J., & Tarjan, R. (1973). Algorithm 447: efficient algorithms for graph manipulation. Communications of the ACM, **16**(6), 372-378.

DOI: http://dx.doi.org/10.1145/362248.362272

Hu, T. C. (1961). Letter to the editor—the maximum capacity route problem. Operations Research, **9**(6), 898-900.

DOI: https://doi.org/10.1287/opre.9.6.898

Kantz, H., & Schreiber, T. (2004). Nonlinear time series analysis (Vol. 7). Cambridge University Press.

Kennel, M. B., Brown, R., & Abarbanel, H. D. (1992). Determining embedding dimension for phase-space reconstruction using a geometrical construction. Physical Review A, **45**(6), 3403.

DOI: https://doi.org/10.1103/PhysRevA.45.3403

Krakovská, A., Mezeiová, K., & Budáčová, H. (2015). Use of false nearest neighbours for selecting variables and embedding parameters for state space reconstruction. Journal of Complex Systems, 2015.

DOI: http://dx.doi.org/10.1155/2015/932750

Liebert, W., & Schuster, H. G. (1989). Proper choice of the time delay for the analysis of chaotic time series. Physics Letters A, **142**(2-3), 107-111.

DOI: https://doi.org/10.1016/0375-9601(89)90169-2

Luce, R. D., & Perry, A. D. (1949). A method of matrix analysis of group structure. Psychometrika, **14**(2), 95-116.

DOI: https://doi.org/10.1007/BF02289146

Newman, M. E. (2002). Assortative mixing in networks. Physical Review Letters, **89**(20), 208701.

DOI: https://doi.org/10.1103/PhysRevLett.89.208701

Newman, M. E. (2016). Mathematics of networks. The new Palgrave dictionary of economics, 1-8.

DOI: https://doi.org/10.1108/09504120310503827

Packard, N.H., Crutchfield, J.P., Farmer, J.D. and Shaw, R.S., 1980. Geometry from a time series. Physical Review Letters, **45**(9), p.712.

DOI: https://doi.org/10.1103/PhysRevLett.45.712

Pons, P., & Latapy, M. (2006). Computing communities in large networks using random walks. Journal of Graph Algorithms and Applications, **10**(2), 191-218.

DOI: https://doi.org/10.1007/11569596_31

Porter, M. A., Onnela, J. P., & Mucha, P. J. (2009). Communities in networks. Notices of the AMS, **56**(9), 1082-1097.

DOI: https://doi.org/10.0902.3788

Sauer, T., Yorke, J. A., & Casdagli, M. (1991). Embedology. Journal of Statistical Physics, **65**(3-4), 579-616.

DOI: https://doi.org/10.1007/bf01053745

Seidman, S. B. (1983). Network structure and minimum degree. Social Networks, **5**(3), 269-287.

DOI: https://doi.org/10.1016/0378-8733(83)90028-X

Shannon, C. E. (1948). A mathematical theory of communication. Bell System Technical Journal, **27**(3), 379-423.

DOI: https://doi.org/10.1002/j.1538-7305.1948.tb01338.x

Stavroglou, S. K., Pantelous, A. A., Soramaki, K., & Zuev, K. (2017). Causality networks of financial assets. Journal of Network Theory in Finance, **3**(2), 17-67.

DOI: https://doi.org/10.21314/JNTF.2017.029

Stavroglou, S. K., Pantelous, A. A., Stanley, H. E., & Zuev, K. M. (2019). Hidden interactions in financial markets. Proceedings of the National Academy of Sciences of the U.S.A., **116**(22), 10646-10651.

DOI: https://doi.org/10.1073/pnas.1819449116

Takens, F. (1981). Detecting strange attractors in turbulence. In Dynamical systems and turbulence, Warwick 1980 (pp. 366-381). Springer, Berlin, Heidelberg.

DOI: https://doi.org/10.1007/BFb0091924

Watts, D. J., & Strogatz, S. H. (1998). Collective dynamics of 'small-world' networks. Nature, **393**(6684), 440.

DOI: https://doi.org/10.1038/30918

West, D. B. (1996). Introduction to Graph Theory (Vol. 2). Upper Saddle River, NJ: Prentice hall. http://free-journal.umm.ac.id

Whitney, H. (1936). Differentiable manifolds. Annals of Mathematics, **37**(3), 645-680.

DOI: https://doi.org/10.2307/1968482

Zhou, S., & Mondragón, R. J. (2004). The rich-club phenomenon in the Internet topology. IEEE Communications Letters, **8**(3), 180-182.

DOI: https://doi.org/10.1109/LCOMM.2004.823426